JCI The Journal of Clinical Investigation

Casein kinase 1α–dependent feedback loop controls autophagy in RAS-driven cancers

Jit Kong Cheong, … , Andrew Thorburn, David M. Virshup

J Clin Invest. 2015;125(4):1401-1418. https://doi.org/10.1172/JCI78018.

Research Article Oncology

Activating mutations in the *RAS* oncogene are common in cancer but are difficult to therapeutically target. RAS activation promotes autophagy, a highly regulated catabolic process that metabolically buffers cells in response to diverse stresses. Here we report that casein kinase 1α (CK1α), a ubiquitously expressed serine/threonine kinase, is a key negative regulator of oncogenic RAS–induced autophagy. Depletion or pharmacologic inhibition of CK1α enhanced autophagic flux in oncogenic RAS–driven human fibroblasts and multiple cancer cell lines. FOXO3A, a master longevity mediator that transcriptionally regulates diverse autophagy genes, was a critical target of CK1α, as depletion of CK1α reduced levels of phosphorylated FOXO3A and increased expression of FOXO3A-responsive genes. Oncogenic RAS increased CK1α protein abundance via activation of the PI3K/AKT/mTOR pathway. In turn, elevated levels of CK1α increased phosphorylation of nuclear FOXO3A, thereby inhibiting transactivation of genes critical for RAS-induced autophagy. In both RAS-driven cancer cells and murine xenograft models, pharmacologic CK1α inactivation synergized with lysosomotropic agents to inhibit growth and promote tumor cell death. Together, our results identify a kinase feedback loop that influences RAS-dependent autophagy and suggest that targeting CK1α-regulated autophagy offers a potential therapeutic opportunity to treat oncogenic RAS–driven cancers.

Casein kinase 1α–dependent feedback loop controls autophagy in RAS-driven cancers

Jit Kong Cheong,[1] Fuquan Zhang,[1] Pei Jou Chua,[2] Boon Huat Bay,[2] Andrew Thorburn,[3] and David M. Virshup[1,4,5]

[1]Cancer and Stem Cell Biology Program, Duke-NUS Graduate Medical School, Singapore. [2]Department of Anatomy, National University of Singapore (NUS), Singapore. [3]Department of Pharmacology, University of Colorado School of Medicine, Aurora, Colorado, USA. [4]Department of Biochemistry, NUS, Singapore. [5]Department of Pediatrics, Duke University School of Medicine, Durham, North Carolina, USA.

Activating mutations in the *RAS* oncogene are common in cancer but are difficult to therapeutically target. RAS activation promotes autophagy, a highly regulated catabolic process that metabolically buffers cells in response to diverse stresses. Here we report that casein kinase 1α (CK1α), a ubiquitously expressed serine/threonine kinase, is a key negative regulator of oncogenic RAS–induced autophagy. Depletion or pharmacologic inhibition of CK1α enhanced autophagic flux in oncogenic RAS–driven human fibroblasts and multiple cancer cell lines. FOXO3A, a master longevity mediator that transcriptionally regulates diverse autophagy genes, was a critical target of CK1α, as depletion of CK1α reduced levels of phosphorylated FOXO3A and increased expression of FOXO3A-responsive genes. Oncogenic RAS increased CK1α protein abundance via activation of the PI3K/AKT/mTOR pathway. In turn, elevated levels of CK1α increased phosphorylation of nuclear FOXO3A, thereby inhibiting transactivation of genes critical for RAS-induced autophagy. In both RAS-driven cancer cells and murine xenograft models, pharmacologic CK1α inactivation synergized with lysosomotropic agents to inhibit growth and promote tumor cell death. Together, our results identify a kinase feedback loop that influences RAS-dependent autophagy and suggest that targeting CK1α-regulated autophagy offers a potential therapeutic opportunity to treat oncogenic RAS–driven cancers.

Introduction

Cancer is one of the leading causes of death worldwide, and the global mortality from cancer is projected to continue rising, with an estimated 12 million deaths in 2030 (1). Activating mutations in the *RAS* oncogene occur in 20%–25% of all human tumors and up to 90% of specific tumor types (2). Oncogenic RAS activation can lead variously to survival, senescence, or death or to cell cycle arrest depending on the genetic status and environment of the cell. One consequence of RAS mutation is the activation of autophagy (3–8). Autophagy is an evolutionarily conserved and highly regulated catabolic process that supports metabolic and biosynthetic programs in response to nutrient deprivation and other forms of stress. In cancers with activating RAS mutations, enhanced autophagy supports the maintenance of lipid homeostasis, mitochondrial metabolism, and nutrient recycling required for robust cell growth (4–7, 9). Oncogenic RAS–driven invasion of cancer cells into surrounding tissues is also critically dependent on autophagy, which promotes basal extrusion (8) and secretion of the promigratory cytokine IL-6 (10). Inhibition of autophagy by genetic means or exposure to lysosomotropic agents such as chloroquine (CQ) can result in regression of tumor xenografts in mice (7), indicating that oncogene-induced autophagy can be indispensable for cancer cell survival in some settings. Excessive autophagy may also lead to cell death by indiscriminate degradation of critical cell survival proteins (3, 11).

A growing number of clinical trials have been conducted to investigate whether inhibition of autophagic recycling by hydroxychloroquine (HCQ) or CQ can sensitize cancer cells to various types of anticancer drugs (12–17). Given that autophagy plays context-dependent roles in cancer, the clinical benefits of targeting autophagy may be unpredictable. Consistent with this concern, a recent study showed that RAS mutation status alone might be insufficient to predict autophagy addiction and CQ sensitivity of cancer cells cultured in vitro (18). Hence, there is a need to define the optimum cellular contexts or identify new biomarkers that will aid in the therapeutic targeting of autophagy via lysosomotropic agents such as CQ or HCQ.

The signaling networks that regulate the degree of autophagic flux remain poorly understood. During a recent study of casein kinase 1 (CK1) in the regulation of cancer cell growth (19), we noted a role for CK1α in the modulation of oncogenic RAS–induced autophagic flux. This observation is consistent with a recent kinome RNAi screen that identified CK1 isoforms as constitutive autophagy-regulating kinases in human breast cancer cells (20). The CK1 family of ubiquitously expressed serine/threonine kinases consists of six human isoforms (α, δ, ε, γ1, γ2, and γ3) that are evolutionary conserved within eukaryotes (21, 22). CK1 isoforms regulate diverse cellular processes including circadian rhythms, WNT signaling, cell transformation, membrane trafficking, cytoskeleton maintenance, DNA replication, DNA damage response, and RNA metabolism (21, 23–26). Unlike its pro-onco-

▶ Related Commentary: p. 1393

Authorship note: Jit Kong Cheong and Fuquan Zhang contributed equally to this work.
Note regarding evaluation of this manuscript: Manuscripts authored by scientists associated with Duke University, The University of North Carolina at Chapel Hill, Duke-NUS, and the Sanford-Burnham Medical Research Institute are handled not by members of the editorial board but rather by the science editors, who consult with selected external editors and reviewers.
Conflict of interest: The authors have declared that no conflict of interest exists.
Submitted: July 21, 2014; **Accepted:** January 28, 2015.
Reference information: *J Clin Invest*. 2015;125(4):1401–1418. doi:10.1172/JCI78018.

genic δ, ε, and γ isoforms, CK1α is thought to be largely antiproliferative. CK1α is a component of the β-catenin destruction complex that normally downregulates WNT signaling (27), as well as a negative regulator of the p53 tumor suppressor (28).

Using genetically engineered variants of human BJ foreskin fibroblasts that mimic key stages of oncogenic H-RAS^{V12}–induced tumorigenesis (29), we investigated whether CK1α regulates basal autophagy induced by oncogenic H-RAS^{V12}. Here we describe a pathway for regulation of RAS-induced basal autophagy, whereby the RAS/PI3K/AKT/mTOR signaling axis upregulates CK1α protein abundance. CK1α in turn phosphorylates and decreases nuclear FOXO3A protein abundance, thereby reducing FOXO3A-mediated transactivation of autophagy-related genes. We found that inhibitors of CK1α and autophagy combine in vitro and in vivo to block cancer progression, illustrating that balanced RAS-driven autophagy is critical for proliferation. These findings offer insights into autophagy regulation and therapeutic combinations that are effective in RAS-driven cancers.

Results

CK1α suppresses RAS-induced basal autophagy. Oncogenic RAS increases basal autophagy to facilitate tumorigenesis (3–7). We confirmed this finding by demonstrating that microtubule-associated protein 1 light chain 3B-II (LC3B-II) protein abundance was upregulated upon 4-hydroxytamoxifen–induced (4-OHT–induced) activation of ER:H-RAS^{V12} (estrogen receptor–fused H-RAS bearing the activating G12V mutation) (Figure 1A). Notably, we also observed an increase in CK1α protein abundance upon activation of ER:H-RAS^{V12} (Figure 1A). To test whether CK1α is involved in the regulation of RAS-induced basal autophagy, we depleted endogenous CK1α with two independent siRNAs. CK1α knockdown produced a marked increase in LC3B-II protein abundance that was dependent on the presence of activated ER:H-RAS^{V12} (Figure 1B versus Supplemental Figure 1A; supplemental material available online with this article; doi:10.1172/JCI78018DS1). Although p53 has been reported to regulate LC3B expression (30), CK1α depletion induced accumulation of LC3B-II even in the absence of p53 (Supplemental Figure 1B). This effect was not cell type specific, as knockdown of CK1α increased LC3B-II protein abundance in oncogenic RAS–driven HCT-116 human colon carcinoma cells as well (Figure 1C). Thus, CK1α inhibits basal autophagy in an oncogenic RAS–specific manner.

CK1α is a member of a family of related serine/threonine kinases. Regulation of RAS-induced autophagy is specific to CK1α, as siRNA-mediated depletion of CK1δ or CK1ε (Figure 1C) or inhibition of their kinase activity by potent small molecules (Supplemental Figure 1C) did not substantially alter LC3B-II protein abundance. Consistent with the knockdown data, pharmacological inhibition of CK1α by D4476 (31, 32) also increased LC3B-II protein levels in the oncogenic RAS–expressing BJ fibroblasts (Figure 1D), as well as in multiple RAS-driven cancer cell lines of diverse human tissue origins (Figure 1E). Thus, CK1α kinase activity is required for the regulation of oncogenic RAS–induced LC3B-II protein accumulation. Conversely, moderate ectopic overexpression of CK1α reduced LC3B-II protein abundance only in oncogenic RAS–expressing BJ fibroblasts (Figure 1F). Similarly, the siCK1α-induced increase in LC3B-II protein abundance was rescued by re-expression of siRNA-resistant CK1α (Supplemental Figure 1D). Given that oncogenic H-RAS^{V12} activates endoplasmic reticulum (ER) stress–associated unfolded protein response (UPR) via upregulation of activating transcription factor 4 (ATF4) and glucose-regulated protein, 78kDa (GRP78/BiP) (33) and that ER stress is a potent inducer of autophagy via upregulation of LC3 (34), we tested whether CK1α depletion or inhibition further upregulates key ER stress factors. Expression of ATF4, growth arrest and DNA damage–inducible protein 34 (GADD34), and GRP78/BiP was examined in the isogenic human colon cancer cells HCT-116$^{K\text{-}RAS\ WT/mutant}$ and HCT-116$^{K\text{-}RAS\ WT/-}$, where the mutant *K-RAS^{G13D}* allele has been knocked out by homologous recombination (35). Neither mutant K-RAS nor CK1α depletion or inhibition induced these ER stress factors, while the positive control thapsigargin (TG) was highly active (Supplemental Figure 1, E and F). Hence, CK1α modulation does not upregulate LC3B-II protein abundance by triggering ER stress responses.

We next determined whether CK1α inhibition upregulates the unbound pool of cytoplasmic LC3B-II or the autophagic vesicle– and autophagosome-bound pool of LC3B-II. Endogenous LC3B-II–associated autophagosomes increased significantly when CK1α was depleted by siRNA or inhibited by D4476 (Figure 1, G and H, and Supplemental Figure 2, A and B). Consistent with the inhibitory role of CK1α, siRNA-mediated depletion of DDX3, a recently characterized activator of CK1α (36), also led to substantial upregulation of endogenous LC3B-II–associated autophagosomes in HCT-116 cells (Supplemental Figure 2C).

p62 (encoded by *SQSTM1*) is an integral part of the autophagosome-lysosome degradation pathway, where it targets polyubiquitinated protein aggregates and dysfunctional organelles to LC3-II–associated autophagosomes (37). Increased p62 correlates well with inhibition of autophagy in mammals and *Drosophila*, indicating that steady-state levels of p62 reflect the autophagic status (37). p62 is downregulated upon CK1α depletion in BJ fibroblasts with activated ER:H-RAS^{V12} (Supplemental Figure 2D), consistent with the CK1α inhibition of RAS-induced autophagic events. To confirm this finding, we examined autophagic flux in HCT-116$^{K\text{-}RAS\ WT/mutant}$ and HCT-116$^{K\text{-}RAS\ WT/-}$ cells by combining CK1α knockdown with exposure to the lysosomotropic agent CQ (37). Depletion of CK1α significantly increased basal LC3B-II abundance, as well as autophagic flux in isogenic mutant K-RAS, but not WT K-RAS, HCT-116 cells (Figure 2A). Importantly, inactivation of CK1α in multiple mutant, but not WT, K-RAS–expressing cancer cell lines also increased basal LC3B-II abundance and autophagic flux (Figure 2B).

Identification of a FOXO3 autophagy gene transactivation signature in CK1α depletion or inhibition. To investigate how CK1α inhibits RAS-induced autophagy, we examined the expression of an array of 84 key autophagy-related genes in oncogenic RAS–driven HCT-116 colon carcinoma cells and T24 bladder carcinoma cells after CK1α knockdown (Figure 3A, Supplemental Figure 3A, and Supplemental Tables 1 and 2). 32% (in HCT-116 cells) and 64.3% (in T24 cells) of autophagy-related genes were transcriptionally upregulated upon CK1α depletion (Figure 3A). Next, we compared the upregulated autophagy-related genes in CK1α-depleted HCT-116 and T24 cells to determine common targets that CK1α may regulate. We identified 21 autophagy-re-

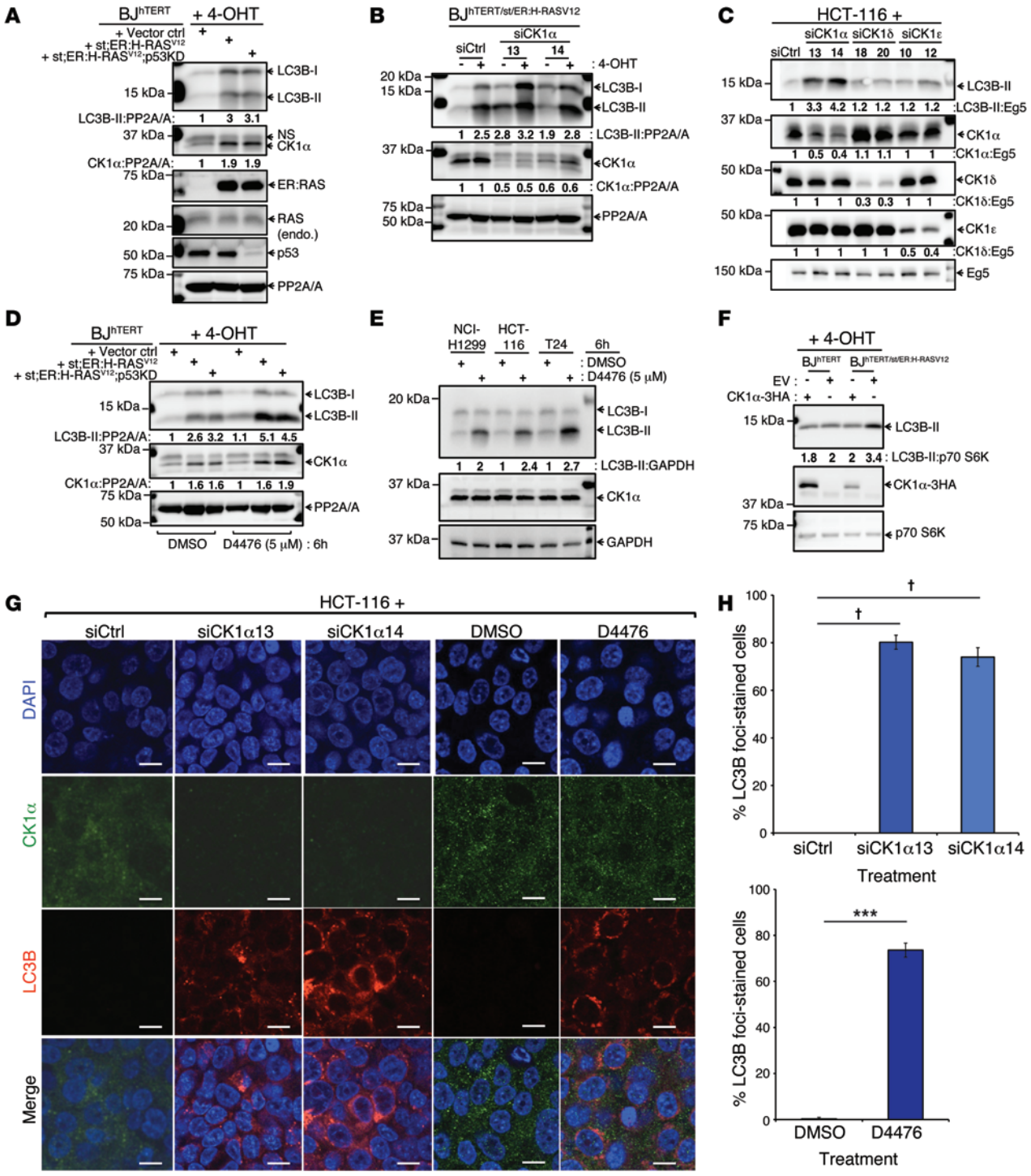

Figure 1. CK1α suppresses RAS-induced basal autophagy. (**A**) LC3B and CK1α are upregulated in BJ fibroblasts with oncogenic H-RAS^{V12}, regardless of p53 status. Cells were treated with 4-OHT for 48 hours. endo, endogenous. (**B**) CK1α depletion further upregulates LC3B-II. Eight hours after siRNA transfection, 4-OHT was added to cells for an additional 72 hours. (**C**) CK1α knockdown specifically increases LC3B-II levels. Cells were analyzed 48 hours after RNAi treatment. (**D**) D4476 potently increases LC3B-II levels in a mutant RAS–specific manner. Forty-eight hours after 4-OHT treatment, cell were incubated with DMSO or D4476 for an additional 6 hours. (**E**) D4476 increases LC3B-II in multiple RAS-mutant cell lines. Cells were treated with DMSO or D4476 (6 hours). (**F**) CK1α overexpression downregulates RAS-induced LC3B-II expression. Cells were transfected with pcDNA3.1 (EV, empty vector) or pcDNA3.1-CK1α-3HA. (**G**) CK1α inhibition increases LC3B-II–associated autophagosomes. Cells were exposed to the indicated siRNAs, DMSO, or D4476 (6 hours). Representative immunofluorescence images from three independent experiments are shown. DAPI stains the nuclei. Scale bars: 20 μm. (**H**) Quantification of LC3B foci–stained cells from **G**, using MetaMorph software (mean ± SD). One-way ANOVA with Dunnett's test (for RNAi treatment) and Student's *t* test (for drug treatment) were used to analyze statistical significance; ***$P < 0.001$; †$P < 0.0001$. Values are mean ± SD from 3 independent experiments. Fold expression change in the proteins of interest after normalization is indicated below protein blots. NS, nonspecific; hTERT, human telomerase catalytic subunit; st, SV40 small t antigen.

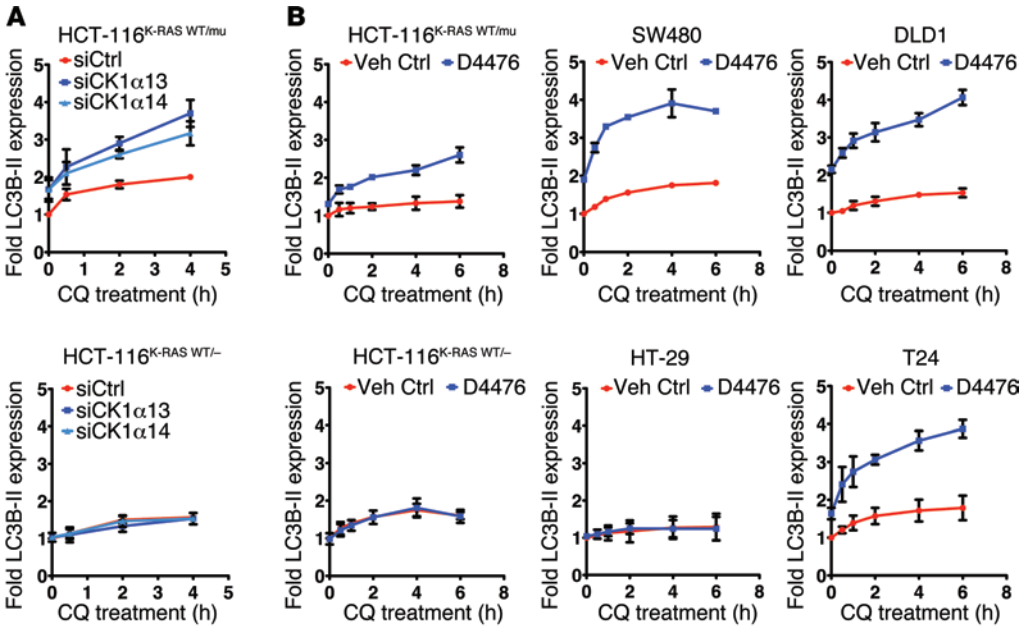

Figure 2. CK1α knockdown or inactivation elevates basal autophagy and autophagic flux in a mutant RAS–dependent manner. (**A**) CK1α depletion increases basal autophagy and autophagic flux in isogenic HCT-116 cells (with/without mutant K-RAS). Cells were analyzed 48 hours after RNAi treatment. (**B**) CK1α inhibition increases basal autophagy and autophagic flux in a mutant RAS–specific manner. Cells were exposed to vehicle control (Veh Ctrl; DMSO) or 5 μM D4476 for 6 hours. Fold change in LC3B-II protein expression after CQ addition over the indicated duration was assessed without or with CK1α knockdown (**A**) or without or with CK1α inhibition (**B**). Values are mean ± SD from 3 independent experiments. Fold expression change in the proteins of interest after normalization is indicated below protein blots. mu, mutant. Cell lines with mutant RAS: SW480, DLD-1, HCT-116$^{K\text{-}RAS\ WT/mu}$, and T24; with WT K-RAS: HT-29 and HCT-116$^{K\text{-}RAS\ WT/-}$.

lated genes that are upregulated in both HCT-116 and T24 cells when CK1α was depleted (Figure 3B). Among these 21 autophagy-related genes, we noted that the expression of *MAP1LC3A* (*LC3A*), *MAP1LC3B* (*LC3B*), *ATG4B*, *ATG12*, *GABARAP*, *GABARAPL1*, *GABARAPL2*, *ULK2*, and *BNIP3* have been previously shown to be directly regulated by the FOXO3 transcription factor (38–40). Transcriptionally competent FOXO3 promotes autophagy in various cell types by increasing the expression of these autophagy core machinery genes (41). To validate our quantitative real-time PCR (qPCR) array data, we designed separate sets of primers that anneal to transcripts of *LC3B*, *BNIP3*, *ATG12*, and *GABARAP* and performed qPCR analyses to probe for changes in their abundance. We confirmed that these transcripts were indeed upregulated when CK1α was depleted by two independent siRNAs in both HCT-116 and T24 cells (Figure 3C). Pharmacological inhibition of CK1α and knockdown of the CK1 activator DDX3 similarly upregulated the same FOXO3-responsive genes (Figure 3D and Supplemental Figure 3B).

FOXO3, a key effector of autophagy, is a bona fide CK1α substrate. The data suggest that CK1α regulates the expression of FOXO3-dependent autophagy genes. We next asked whether CK1α directly regulates FOXO3A, the predominant form of FOXO3 expressed in cells. FOXO3A contains a putative CK1 phosphorylation motif, pS/pT-X-X-S/T (where pS/pT refers to a phospho-serine/phospho-threonine, and X refers to any amino acid). ClustalW multiple sequence alignment revealed that this CK1 phosphorylation motif is present in all FOXO isoforms except FOXO6, and it is evolutionarily conserved across different species (Figure 4A and Supplemental Figure 4A).

FOXO1 has been previously shown to be a CK1 substrate in vitro (32), but it is not known which CK1 isoforms regulate the FOXO transcription factors in the cell. Hence, we tested whether CK1α can phosphorylate FOXO3A in vivo. To facilitate analysis, we used human embryonic kidney 293 (HEK293) cells that have low amounts of endogenous FOXO3A. We verified that a commercially available phospho-FOXO3A$^{S318/321}$ antibody reacted with the wild-type but not FOXO3A$^{S318/321A}$ mutant protein (Figure 4B, lanes 4–6). CK1α depletion significantly reduced phosphorylation of ectopically expressed FOXO3A at S318/321, consistent with it being an in vivo FOXO3A kinase (Figure 4B, lanes 1–3). CK1 preferentially phosphorylates primed substrates, and priming phosphorylation of the related FOXO1^{S319} by AKT is critical for CK1δ-dependent FOXO1 phosphorylation (32, 42). Given that this priming serine residue is conserved among members of the FOXO family (Figure 4A), we tested whether AKT phosphorylation at FOXO3A^{S315} is required for CK1α-dependent FOXO3A$^{S318/321}$ phosphorylation. We expressed the FOXO3A^{S315A} mutant in HEK293 cells and found that it phenocopies the loss of CK1α phosphorylation observed in the alanine mutants of FOXO3A$^{S318/321}$ (Supplemental Figure 4B), supporting the notion that FOXO3A^{S315} phosphorylation by AKT primes subsequent CK1α phosphorylation of FOXO3A$^{S318/321}$. AKT-dependent phosphorylation at FOXO3A^{S315}, not FOXO3A^{T32} or FOXO3A^{S253}, results in the mobility shift of FOXO3A in protein gels (40). Mutation of the downstream phosphorylation sites at FOXO3A$^{S318/321}$ similarly disrupted the phosphorylation-associated mobility shift in protein gels caused by coexpression with constitutively active HA-tagged AKT (HA-AKT-CA) (Supplemental Figure 4B).

CK1α depletion led to decreased FOXO3A$^{S318/321}$ phosphorylation and an accumulation of endogenous total FOXO3A proteins in both HCT-116 and T24 (*RAS*-mutant) cancer cells (Figure 4C and Supplemental Figure 4C). The effect was specific to CK1α, since the abundance of FOXO3A proteins was unaffected by CK1δ or CK1ε depletion (Figure 4C and Supplemental Figure 4C). Consistent with this, the increase in LC3B protein abundance was also specific to CK1α depletion and was unaffected by depletion of CK1δ or CK1ε (Figure 4C and Supplemental Figure 4C). Similar results were obtained when we depleted the CK1α

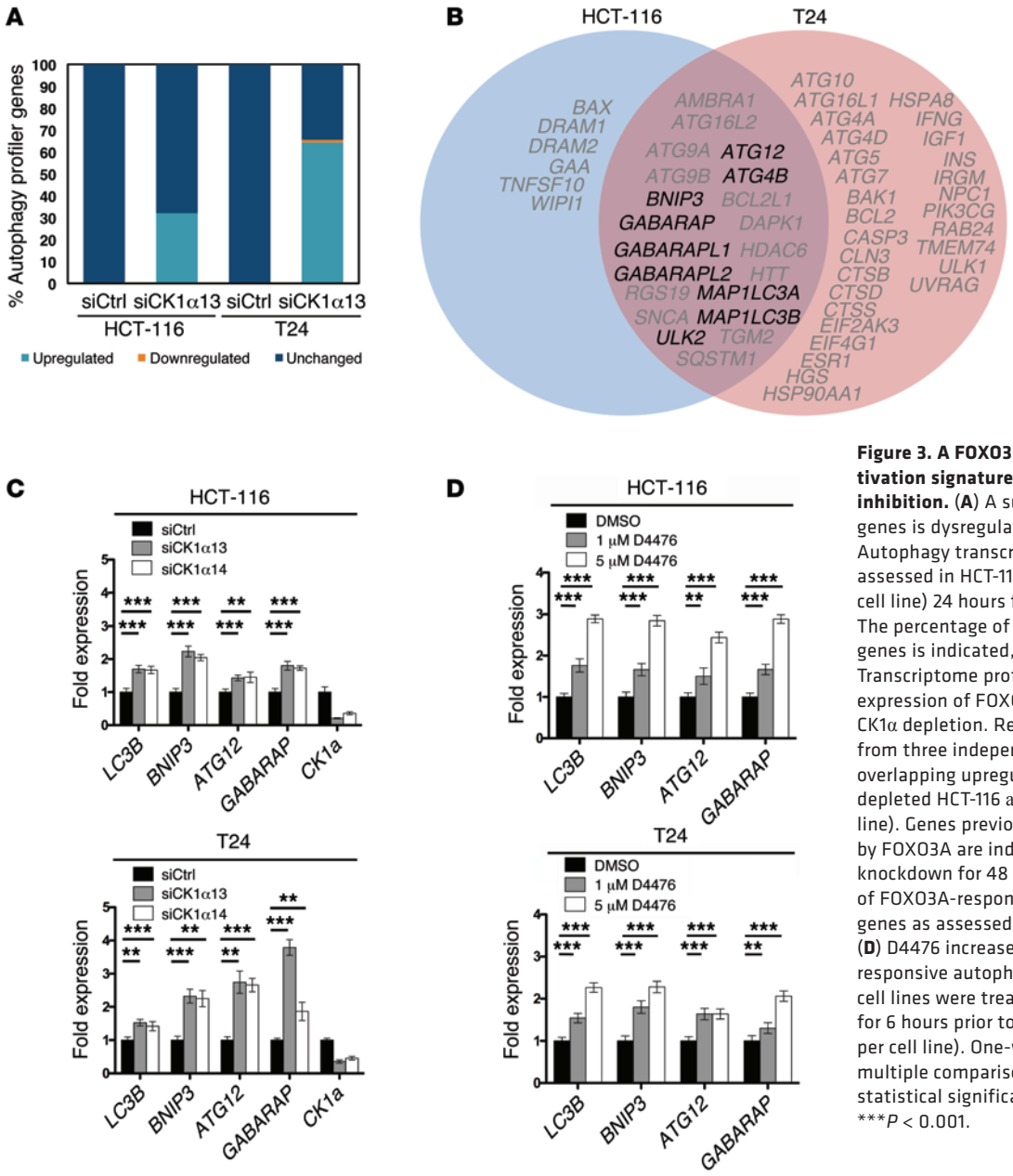

Figure 3. A FOXO3 autophagy gene transactivation signature after CK1α depletion or inhibition. (**A**) A subset of autophagy-related genes is dysregulated upon CK1α depletion. Autophagy transcriptome changes were assessed in HCT-116 and T24 cells (n = 3 per cell line) 24 hours following CK1α knockdown. The percentage of differentially regulated genes is indicated, using a 1.5-fold cut off. (**B**) Transcriptome profiling identifies enhanced expression of FOXO3A-responsive genes upon CK1α depletion. Representative Venn diagram from three independent experiments depicts overlapping upregulated genes in CK1α-depleted HCT-116 and T24 cells (n = 3 per cell line). Genes previously shown to be regulated by FOXO3A are indicated in bold. (**C**) CK1α knockdown for 48 hours increases expression of FOXO3A-responsive autophagy-related genes as assessed by qPCR (n = 3 per cell line). (**D**) D4476 increases expression of FOXO3A-responsive autophagy-related genes. Indicated cell lines were treated with DMSO or D4476 for 6 hours prior to analysis by qPCR (n = 3 per cell line). One-way ANOVA with Dunnett's multiple comparison test was used to analyze statistical significance in **C** and **D**; $^{**}P < 0.01$; $^{***}P < 0.001$.

cofactor DDX3 in HCT-116 and T24 cells via two independent siRNAs (Supplemental Figure 4D). CK1α depletion or inhibition also reduced phosphorylation of FOXO3A at S318 and S321, increased FOXO3A protein stability, and increased LC3B-II protein abundance in isogenic mutant K-RAS, but not wild-type K-RAS–expressing, HCT-116 cancer cells (Figure 4D). Furthermore, the expression of FOXO3A-responsive genes (*LC3B*, *BNIP3*, *ATG12*, and *GABARAP*) increased upon CK1α depletion or inhibition only in mutant RAS–driven HCT-116 cancer cells (Supplemental Figure 4E). Importantly, pharmacological inhibition of CK1α by D4476 similarly reduced FOXO3A$^{S318/321}$ phosphorylation and increased FOXO3A accumulation in both HCT-116 and T24 cells in a dose-dependent manner (Figure 4E and Supplemental Figure 4F). CK1α regulation of FOXO3A appears to be dependent on mutant RAS, since D4476 blockade of CK1α activity did not alter FOXO3A phosphorylation or abundance in WT RAS-expressing HCT-116 (Figure 4D) or HT-29 colon cancer cells (Figure 4E). Thus, CK1α regulates FOXO3A, the key regulator of early autophagy-related gene transactivation.

We examined the consequences of CK1α phosphorylation of FOXO3A. The nuclear pool of FOXO3A protein was elevated following CK1α depletion (Figure 4F), coincident with upregulation of LC3B-II proteins (Figure 4F). Similar increases in nuclear FOXO3A were seen when CK1α was pharmacologically inhibited by D4476 (Figure 4G and Supplemental Figure 4G). Conversely, activation of CK1α with the allosteric activator pyrvinium pamoate (Pyr Pam) (43) downregulated nuclear FOXO3A and led to a decrease in cytoplasmic LC3B-II proteins (Figure 4G and Supplemental Figure 4G). Notably, changes in nuclear FOXO3A abundance were not accompanied by reciprocal changes in FOXO3A cytoplasmic abundance, suggesting that CK1α regulates the protein stability, rather than the nuclear export, of FOXO3A.

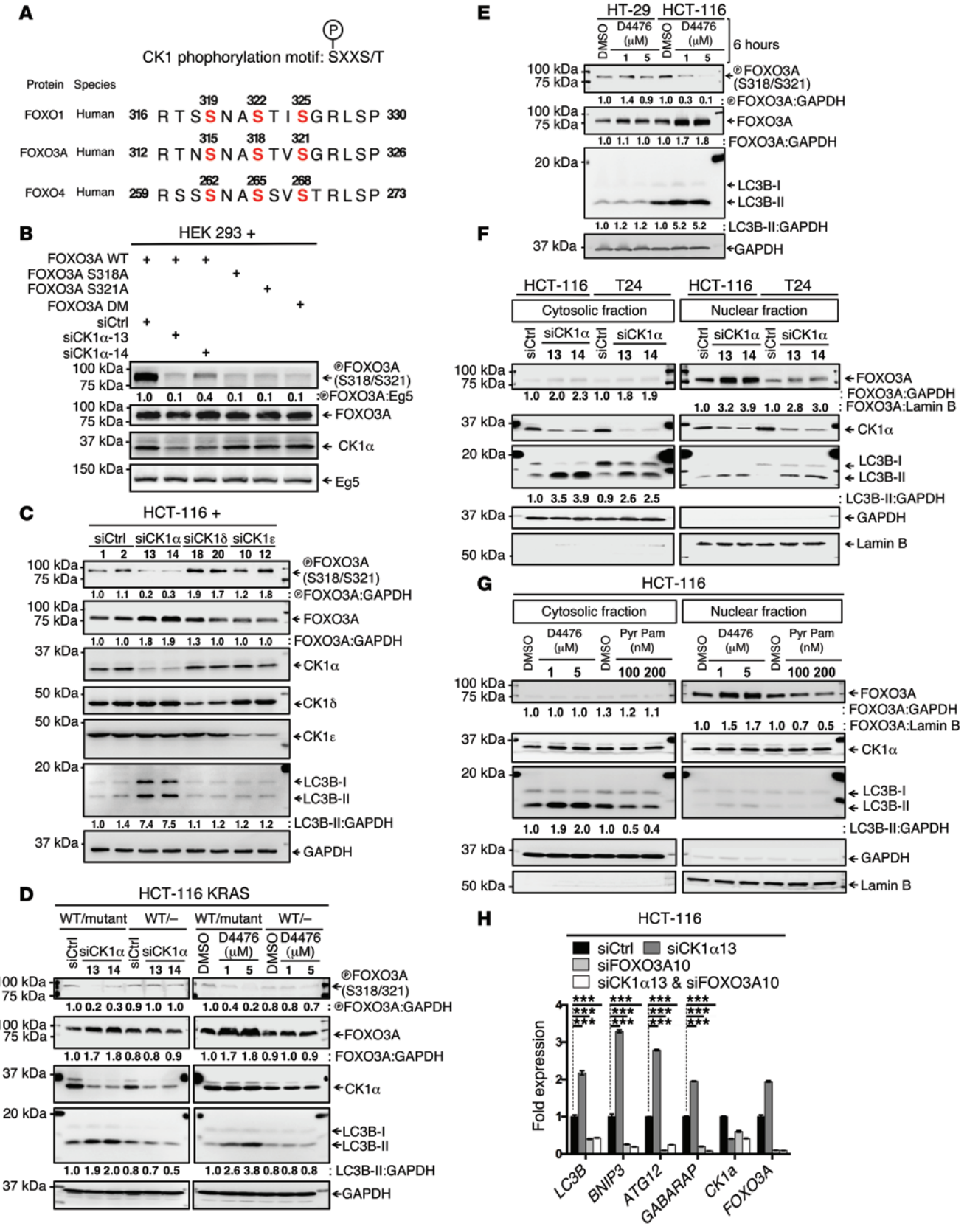
A
CK1 phophorylation motif: SXXS/T
Protein Species
FOXO1 Human 316 R T S S N A S T I S G R L S P 330
FOXO3A Human 312 R T N S N A S T V S G R L S P 326
FOXO4 Human 259 R S S S N A S S V S T R L S P 273
B
HEK 293 +
FOXO3A WT
FOXO3A S318A
FOXO3A S321A
FOXO3A DM
siCtrl
siCK1α-13
siCK1α-14
FOXO3A (S318/S321)
FOXO3A:Eg5
FOXO3A
CK1α
Eg5
C
HCT-116 +
siCtrl siCK1α siCK1δ siCK1ε
FOXO3A (S318/S321)
FOXO3A:GAPDH
FOXO3A
CK1α
CK1δ
CK1ε
LC3B-I
LC3B-II
LC3B-II:GAPDH
GAPDH
D
HCT-116 KRAS
WT/mutant WT/–
siCtrl siCK1α DMSO D4476 (μM)
FOXO3A (S318/S321)
FOXO3A:GAPDH
FOXO3A
CK1α
LC3B-I
LC3B-II
LC3B-II:GAPDH
GAPDH
E
HT-29 HCT-116
DMSO D4476 (μM)
6 hours
FOXO3A (S318/S321)
FOXO3A:GAPDH
FOXO3A
LC3B-I
LC3B-II
LC3B-II:GAPDH
F
HCT-116 T24
Cytosolic fraction
Nuclear fraction
siCtrl siCK1α
FOXO3A
FOXO3A:GAPDH
FOXO3A:Lamin B
CK1α
LC3B-I
LC3B-II
LC3B-II:GAPDH
GAPDH
Lamin B
G
HCT-116
Cytosolic fraction
Nuclear fraction
DMSO D4476 (μM) Pyr Pam (nM)
FOXO3A
FOXO3A:GAPDH
FOXO3A:Lamin B
CK1α
LC3B-I
LC3B-II
LC3B-II:GAPDH
GAPDH
Lamin B
H
HCT-116
siCtrl
siCK1α13
siFOXO3A10
siCK1α13 & siFOXO3A10
Fold expression
LC3B
BNIP3
ATG12
GABARAP
CK1a
FOXO3A

Figure 4. CK1α phosphorylates FOXO3A to regulate its protein abundance. (**A**) A conserved CK1 phosphorylation motif in FOXO3A. (**B**) CK1α phosphorylates FOXO3A at S318 and S321 in vivo. Twenty-four hours after transfection with the indicated proteins, HEK293 cells were treated with the indicated siRNAs for an additional 48 hours prior analysis. (**C**) CK1α is the only cytoplasmic CK1 isoform that phosphorylates FOXO3A in vivo. CK1 isoforms were depleted with the two indicated independent siRNAs (48 hours) prior to analysis. (**D**) CK1α depletion or inhibition increases FOXO3A protein stability in a mutant K-RAS–dependent manner. Cells were incubated with siCtrl, siCK1α (no. 13 or 14, 48 hours), DMSO, or 5 μM D4476 (6 hours). (**E**) D4476 reduces FOXO3A$^{S318/321}$ phosphorylation but increases total FOXO3A abundance only in mutant RAS-driven cancer cells. HT-29 and HCT-116 cells were treated with DMSO or D4476 (6 hours). (**F**) Knockdown of CK1α upregulates nuclear abundance of FOXO3A. HCT-116 and T24 cells were treated with the indicated siRNAs (48 hours) before analysis. (**G**) Small molecule regulators of CK1α control nuclear abundance of FOXO3A. HCT-116 cells were treated with the indicated compounds (6 hours) prior to analysis. (**H**) FOXO3A is required for CK1α regulation of autophagy genes. The indicated FOXO3A-dependent autophagy genes were assessed by qPCR after CK1α and FOXO3A depletion as indicated. Data are mean ± SD of triplicate experiments. Fold expression change in the proteins of interest after normalization is shown below protein blots. ***$P < 0.001$ by 1-way ANOVA with Dunnett's test.

Next, we investigated whether CK1α requires FOXO3A to stimulate autophagy-related gene expression. Consistent with our earlier data, the expression of *LC3B*, *BNIP3*, *ATG12*, and *GABARAP* transcripts was significantly upregulated when CK1α was depleted in HCT-116 and T24 cancer cells. Knockdown of FOXO3A was sufficient to suppress the expression of *LC3B*, *BNIP3*, *ATG12*, and *GABARAP* (Figure 4H and Supplemental Figure 4H), and co-depletion of CK1α was unable to upregulate these transcripts in the absence of FOXO3A. Importantly, depletion of FOXO3A abolished the CK1α inhibition–induced autophagic flux increase in T24 cancer cells (Supplemental Figure 4I). These data are consistent with CK1α-dependent suppression of RAS-induced autophagy being largely mediated through FOXO3A.

CK1α overexpression or activation downregulates FOXO3A protein abundance and function. We further explored the role of CK1α as a suppressor of RAS-induced autophagy. Ectopic expression of CK1α in both HCT-116 and T24 cells led to a significant reduction in the expression of *LC3B*, *BNIP3*, *ATG12*, and *GABARAP* transcripts (Figure 5A). This correlated well with the loss of LC3B-II protein (Figure 5B and Supplemental Figure 5, A and B). Consistent with the results of CK1α depletion, overexpression of exogenous CK1α increased FOXO3A$^{S318/321}$ phosphorylation and decreased FOXO3A and LC3B-II protein abundance (Figure 5C and Supplemental Figure 5C). The kinase activity of CK1α was required for this regulation of FOXO3A phosphorylation and the protein abundance of FOXO3A and LC3B-II, as the kinase-dead CK1α mutant (K46A) failed to induce these changes (Figure 5C and Supplemental Figure 5C). Similar increases in FOXO3A phosphorylation, downregulation of FOXO3A targets, and decreases in LC3B-II were seen when endogenous CK1α was activated by Pyr Pam (Figure 5, D and E, and Supplemental Figure 5D). Collectively, our data suggest that CK1α kinase activity suppresses RAS-induced basal autophagy by promoting phosphorylation and protein turnover of FOXO3A to downregulate expression of FOXO3A-responsive autophagy-related genes.

The PI3K/mTOR signaling axis regulates CK1α protein abundance in an oncogenic RAS–specific manner. CK1α is thought to be constitutively active due to the absence of an autophosphorylatable carboxyl terminus (21, 27, 44), and little is known about how its expression is regulated. We observed that CK1α protein abundance was elevated upon activation of ER:H-RAS^{V12} in BJ-derived fibroblasts (Figure 1A). When RAS^{V12} was activated in BJ^{hTERT} fibroblasts by addition of 4-OHT, CK1α protein abundance increased in as little at 30 minutes and continued to increase in a time-dependent manner (Figure 6A), while *CK1a* transcripts remained constant (Figure 6B and Supplemental Figure 6A). To test whether this was a general phenomenon, we assessed the abundance of CK1α proteins in the isogenic human colon cancer cells HCT-116$^{K\text{-}RAS\ WT/mutant}$ and HCT-116$^{K\text{-}RAS\ WT/-}$. Consistent with the data in fibroblasts, CK1α protein, but not *CK1a* mRNA, was significantly reduced upon removal of the oncogenic K-RAS (Figure 6C and Supplemental Figure 6, B and C). Furthermore, this effect was specific to CK1α, as no change was seen in CK1δ or CK1ε. Thus, oncogenic RAS appears to specifically regulate CK1α abundance in a post-transcriptional manner.

Oncogenic RAS could increase CK1α protein abundance through several pathways. We inactivated each of the three major RAS signaling effector pathways (RAL/GDS, PI3K/AKT/mTOR, and RAF/MEK/ERK) in BJ$^{hTERT/st/ER:H\text{-}RASV12}$ fibroblasts with the small molecule inhibitors SB203580 (45), LY294002 (46), and U0126 (47). Inhibition of PI3K by LY294002 significantly reduced CK1α protein abundance (Figure 6D). In addition, CK1α protein abundance was downregulated in LY294002-treated BJ$^{hTERT/st/ER:H\text{-}RASV12}$ and HCT-116 cells in a time-dependent manner, with an approximately 50% reduction after 2 hours of drug exposure (Figure 6E). Confirming this is an on-target effect of LY294002, a similar decline in CK1α protein, but not *CK1a* mRNA, abundance was seen upon treatment with an unrelated PI3K inhibitor, BKM120 (Supplemental Figure 6, C and D). CK1α protein abundance was similarly downregulated by two independent mTOR inhibitors, rapamycin and PP242 (Figure 6F and Supplemental Figure 6E). We conclude that the RAS/PI3K/AKT/mTOR pathway is responsible for the post-transcriptional upregulation of CK1α protein.

The combination of D4476-mediated autophagy induction and CQ-induced autophagy inhibition synergistically arrests growth of oncogenic RAS–driven cancers. The data indicate that oncogenic RAS enhances CK1α abundance and hence activity, and this then modulates autophagy. We tested whether disruption of this control mechanism inhibited cancer proliferation. A panel of human cancer cell lines with oncogenic RAS (HCT-116, T24, and NCI-H1299) and WT RAS (PC3 and HeLa) was treated with increasing doses of the CK1α inhibitor D4476 for a total duration of 5 days. The proliferation of the oncogenic RAS–driven cancer cells was moderately sensitive to D4476 in a dose-dependent manner (Supplemental Figure 7A). To assess whether these cancer cells can be further sensitized to CK1 inhibition, we combined CK1α inhibition with CQ treatment to achieve hyperaccumulation of ineffective autophagosomes or autolysosomes in the targeted cancer cells by simultaneous induction of autophagosome biogenesis and blockade of their turnover. Notably, synergistic growth inhibition was achieved when the RAS-driven, but not RAS-WT, cancer cells were treated with the combination of 1 μM D4476 and 5 μM CQ

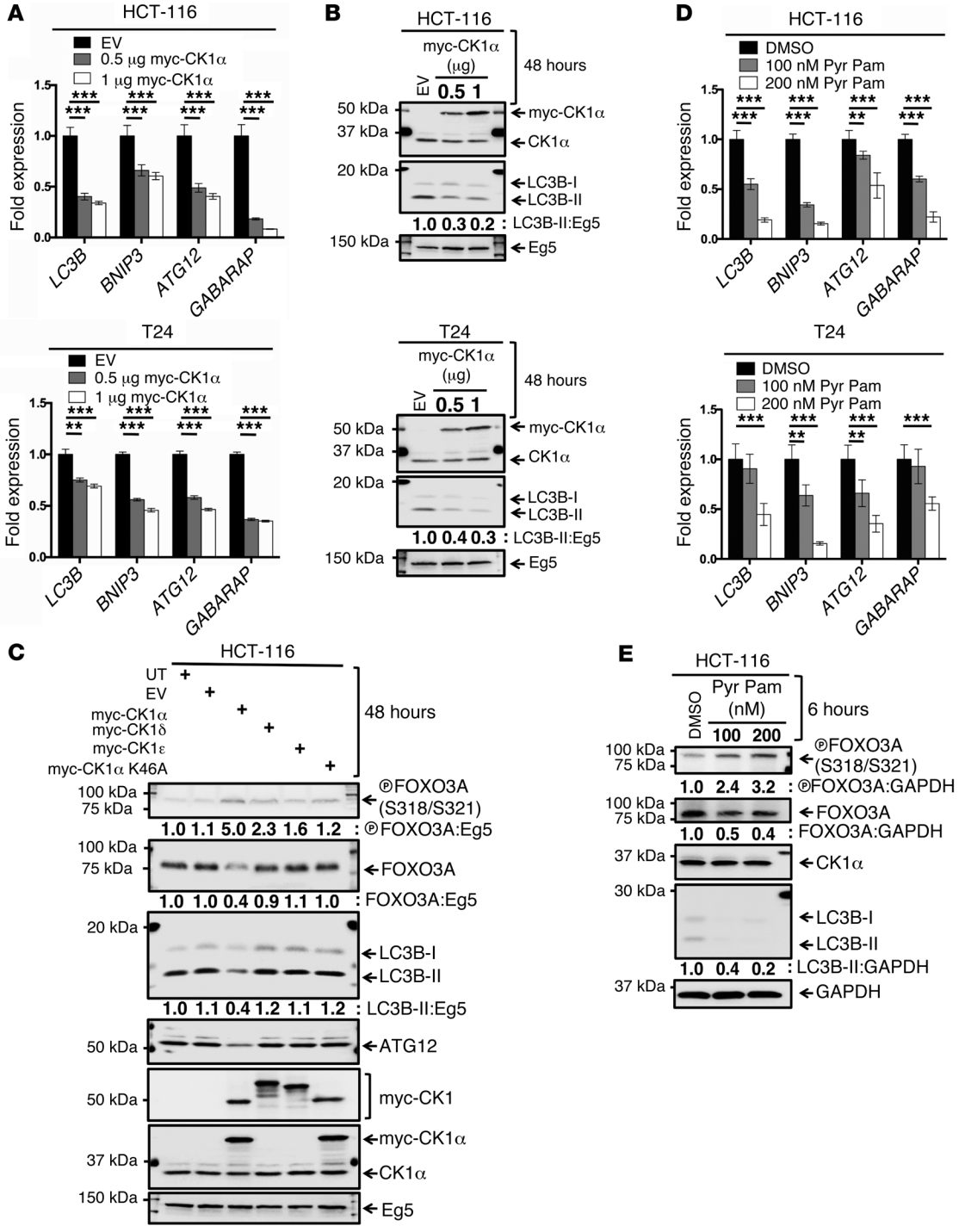

Figure 5. CK1α expression downregulates FOXO3A protein abundance and function. (**A**) CK1α expression reduces expression of FOXO3A-responsive autophagy-related genes. HCT-116 and T24 cells were transfected with pCS2 or pCS2-6MT-CK1α (myc-CK1α) for 48 hours prior to analysis. Data are mean ± SD of triplicate experiments. (**B**) CK1α expression reduces LC3B protein abundance. Lysates from the experiment in **A** were analyzed by immunoblotting for the indicated proteins. (**C**) CK1α kinase activity specifically regulates FOXO3A and autophagy. The indicated proteins were expressed in HCT-116 cells for 48 hours prior to analysis. UT, untransfected. (**D**) CK1α activation by Pyr Pam reduces expression of FOXO3A-responsive genes. HCT-116 and T24 cells were treated for 6 hours as indicated prior to analysis. Data are mean ± SD of triplicate experiments. (**E**) CK1α activation by Pyr Pam increases FOXO3A$^{S318/321}$ phosphorylation and decreases FOXO3A protein abundance. Representative immunoblots of endogenous phospho-FOXO3A$^{S318/321}$, FOXO3A, and LC3B expression in cells from **D**. Fold expression change in the proteins of interest after normalization is shown below protein blots. One-way ANOVA with Dunnett's multiple comparison test was used to analyze statistical significance in **A** and **D**; $^{**}P < 0.01$; $^{***}P < 0.001$.

(D4476:CQ; Figure 7A). Consistent with the synergistic growth inhibition being attributable to blockade of effective autophagy, similar results were obtained when treatment with the lysosomotropic agent ammonium chloride (NH_4Cl) was combined with CK1α inhibition (Supplemental Figure 7B). To determine whether D4476:CQ was indeed synergistic, we subjected mutant RAS–driven HCT-116 and T24 cancer cells to drug combination studies in accordance with the method of Chou and Talalay (48) and calculated combination indices (CIs) at various growth inhibition rates (50%, 75%, and 90%). Synergy, as defined by a CI less than 1 between D4476 and CQ, was observed at all effect levels (Supplemental Figure 7C).

A strategy that targets cancer cells dependent on oncogenic RAS could be of value in cancer therapy. To further test whether activated RAS is required to create autophagy dependency, we tested the drug combinations in the isogenic colon cancer cell lines HCT-116$^{K\text{-}RAS\ WT/mutant}$ and HCT-116$^{K\text{-}RAS\ WT/-}$. The presence of mutant RAS in HCT-116 cells conferred sensitivity to D4476:CQ treatment, since the removal of mutant K-RAS (G13D) rendered HCT-116 cells resistant to D4476:CQ treatment (Figure 7B). We confirmed that short-term exposure (18 hours) to D4476:CQ further upregulated protein abundance of FOXO3A, LC3B-II, and p62 in T24 and HCT-116 cells (Figure 8A), indicative of blockade of effective autophagy in these cells. Importantly, the combination, but neither treatment individually, led to an increase in poly(ADP-ribose) polymerase (PARP) cleavage (Figure 8A), indicating the activation of cell death pathways. HCT-116 cancer cells expressing isogenic mutant, but not WT, K-RAS also exhibited a significant increase in cell death in quantitative flow cytometry analyses (Figure 8B). Together, these findings suggest that D4476:CQ elevated the level of ineffective autophagy to favor cell death specifically in oncogenic RAS–driven cancer cells. Furthermore, knockdown of FOXO3A was sufficient to rescue mutant K-RAS–driven HCT-116 cancer cells from D4476:CQ-induced growth arrest (Figure 8C), indicating that the synergistic interaction of CK1α and lysosomal inhibition requires FOXO3A.

To test whether this drug combination was an effective therapy for mutant RAS–dependent cancers in vivo, we treated mice carrying HCT-116 xenografts with vehicle alone, D4476 (15 mg/kg; hereafter referred to as mpk), CQ (15 mpk), or D4476:CQ (15 mpk:15 mpk) combination daily for 15 days. D4476:CQ synergistically inhibited growth of the tumors (Figure 9, A and B). We similarly tested the drug combination in a T24 xenograft model. Again, the combination of D4476 and CQ was substantially more effective than either agent alone (Supplemental Figure 8A). No weight loss was seen in any treatment conditions, suggesting that the drugs were well tolerated in mice for more than 2 weeks (Supplemental Figure 8, B and C). The HCT-116 tumor xenografts were molecularly assessed at the end of therapy. As predicted, LC3B immunohistochemical staining was significantly upregulated by the drug combination, indicating a defect in autophagy in these tumors (Figure 10A). This is consistent with transmission electron microscopic analysis that revealed an increase in autophagosomes and autolysosomes only in D4476:CQ-treated tumor xenografts (Figure 10B). Similarly, an increase in FOXO3A and LC3B-II protein abundance was seen in the D4476:CQ-treated tumors (Figure 10C). Importantly, we observed an increase in PARP cleavage via Western blot (WB) analysis (Figure 10C) and TUNEL-positive HCT-116 cancer cells (Figure 10D) only in the drug combination–treated xenografts, suggesting the induction of cell death. Consistent with these findings, qPCR profiling of total RNA isolated from these xenografts indicated that the expression of the autophagy-related genes *LC3B*, *BNIP3*, *ATG12*, and *GABARAP* was markedly upregulated by D4476:CQ, indicative of enhanced autophagy (Figure 10E).

Discussion

Autophagy is an evolutionarily conserved waste removal and nutrient recycling mechanism that is activated by various cellular stresses (49), including chronic exposure of oncogene activation during cancer progression. Oncogenic RAS–driven cancer cells elevate basal autophagy to cope with the pressure of rapid growth by maintaining proper mitochondrial homeostasis and recycling biosynthetic intermediates (4–7, 9, 50). In the present study, we uncover a role for CK1α in the regulation of oncogenic RAS–induced basal autophagic flux. Furthermore, our work suggests that modulating the activity of CK1α as a means to target cytoprotective autophagy may stop the progression of many cancers driven by oncogenic RAS. Our findings provide a mechanistic understanding to reports that CK1α inhibition is anti- rather than pro-oncogenic. For example, CK1α knockdown has been reported to impair mutant RAS–driven transformation and growth in plasmocytomas (51). Importantly, we observed that the autophagy induction by CK1α inactivation and autophagy inhibition by lysosomotropic agents (CQ or ammonium chloride) act synergistically to arrest growth of cancer cells of diverse human tissue origins in a mutant RAS–specific manner. Such growth perturbation is not seen in mutant *K-RAS*–null HCT-116 colon cancer cells (Figure 7B) or in HT-29 colon cancer cells with WT *RAS* (Figure 7A). Thus, our data suggest that CK1α may be a tractable enzyme to cotarget with lysosomal inhibition in mutant RAS–driven, autophagy-dependent cancers. The synergy observed with the dual treatment regimen could be the additive result of distinct biological impairments in mutant RAS-driven cancer cells. However, the data are fully consistent with a model whereby CK1α inhibition increases autophagosome formation and subsequent inhibition of the function of those autophagic vesicles by CQ leads to an accumulation of ineffective autophagic vesicles. These accumulating vesicles could promote cell death either by depriving the RAS-stimulated cell of reusable products of proteolysis (Figure 11) or potentially by producing a vesicle-dependent cell death signal. In the first scenario, the combination therapy increases flux of cellular products into a dead end, depriving the cell of factors required for growth, resulting in cell death. In the second scenario, which is not mutually exclusive, a buildup of vesicles might itself serve as a cell death signal by a currently unknown mechanism. Consistent with this latter model, we found that knockdown of FOXO3A blocked increased autophagy and hence autophagic recycling, yet this restored cell proliferation (Figure 8C). In either case, this combination therapy may be striking directly at an Achilles heel of RAS-driven cancers.

A recent kinome RNAi screen scored CK1α as a significant basal autophagy-regulating kinase in MCF-7 human breast cancer cells (20). In that study, the authors attributed the enhancement

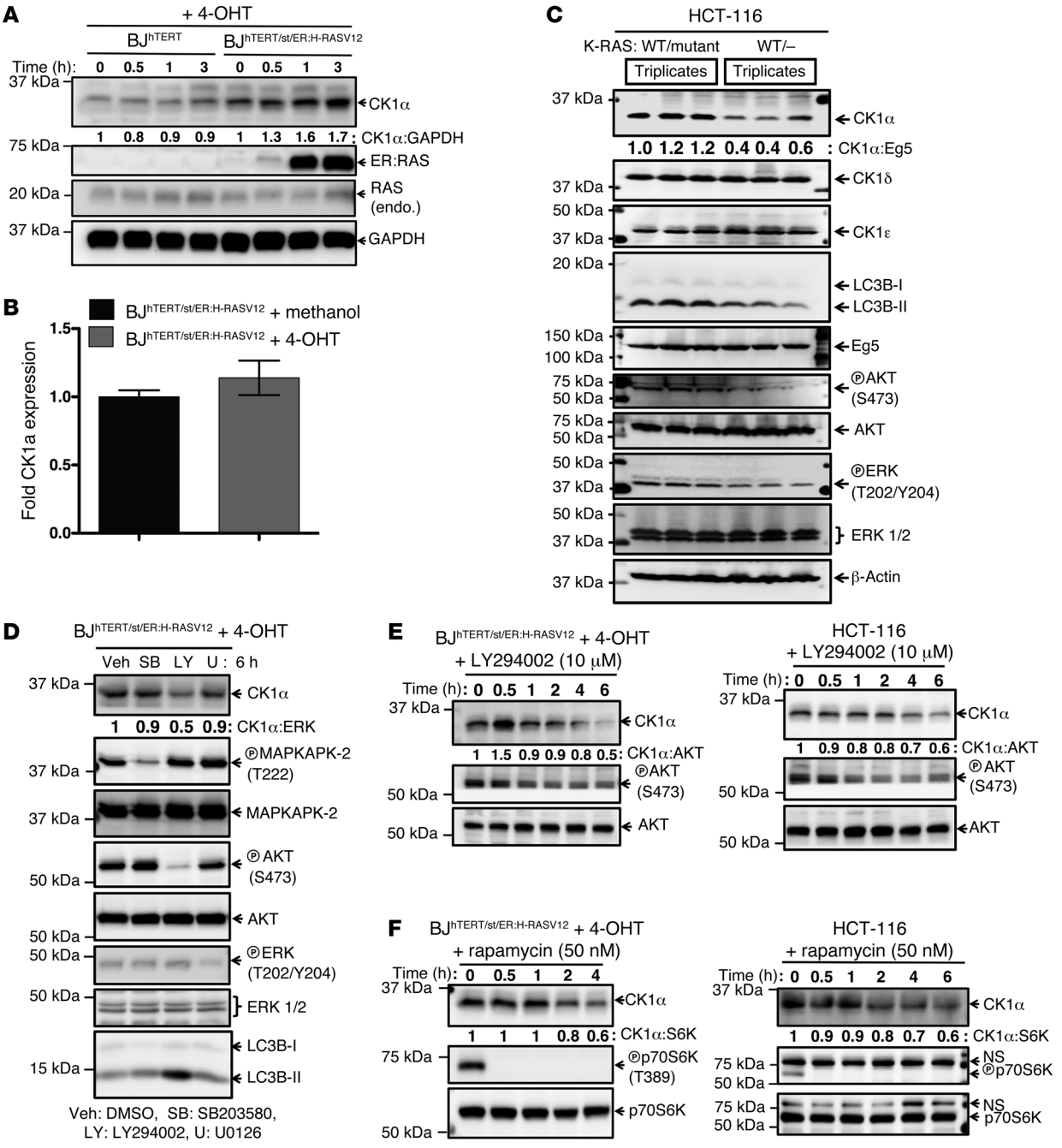

Figure 6. The PI3K/mTOR signaling axis regulates CK1α protein abundance upon RAS activation. (**A**) Activation of oncogenic H-RAS^{V12} increases CK1α protein abundance in a time-dependent manner. BJ-derived fibroblasts were exposed to 4-OHT for the indicated times. (**B**) *CSNK1A1* (*CK1a*) transcript abundance as assessed by qPCR was unchanged by H-RAS^{V12} activation for 24 hours. (**C**) Loss of oncogenic RAS decreases CK1α protein abundance and autophagy. Isogenic HCT-116 cells (with or without mutant K-RAS) were analyzed by immunoblotting with the indicated antibodies. (**D**) Blockade of PI3K activity reduces CK1α protein abundance. BJ$^{hTERT/st/ER:H\text{-}RASV12}$ fibroblasts were exposed to 130 nM 4-OHT for 24 hours. Eighteen hours after the start of 4-OHT treatment, DMSO (Veh), SB203580 (SB; 10 μM), LY294002 (LY; 10 μM), or U0126 (U; 10 μM) was added to the cells for a further 6 hours of incubation prior to analysis by immunoblotting. (**E**) LY294002 reduces CK1α protein abundance in a time-dependent manner. Representative immunoblots of endogenous CK1α protein expression in BJ$^{hTERT/st/ER:H\text{-}RASV12}$ and HCT-116 cells treated with LY294002 for the indicated times. (**F**) Rapamycin reduces CK1α protein abundance in a time-dependent manner. Representative immunoblots of endogenous CK1α protein expression in BJ$^{hTERT/st/ER:H\text{-}RASV12}$ and HCT-116 cells treated with rapamycin for the indicated times. Fold expression change in the proteins of interest after normalization is shown below protein blots.

of autophagic flux following CK1α depletion to increased proteolytic activity of lysosomal hydrolases such as cysteine cathepsins through an unidentified mechanism. Our data indicate that CK1α functions via the master longevity mediator and key transcription factor of autophagy gene transactivation FOXO3A. The AKT-dependent priming phosphorylation at FOXO3A^{S315} is required for subsequent CK1α-dependent phosphorylation of FOXO3A^{S318} and FOXO3A^{S321}. These AKT-CK1α–mediated phosphorylations

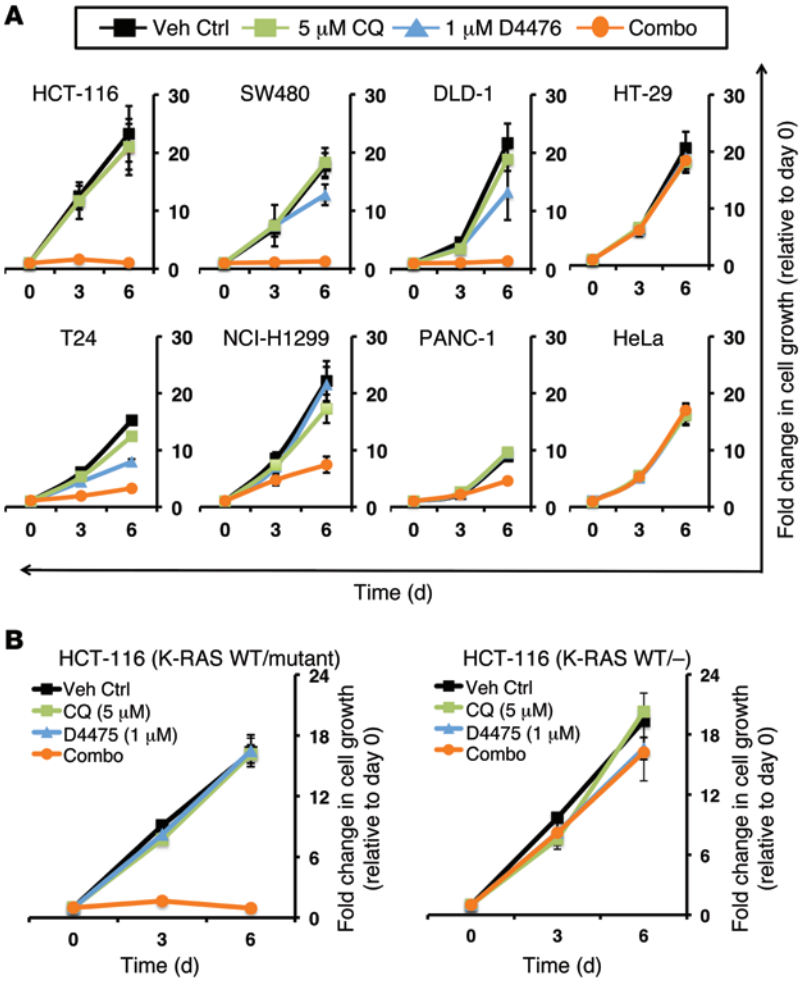

Figure 7. CK1α inhibition synergizes with lysosomal inhibition to arrest growth of RAS-driven human cancer cells. (**A**) RAS-driven cancer cells are sensitive to D4476:CQ (Combo) treatment. Human cancer cell lines (n = 3 per cell line) with mutant RAS (HCT-116, SW480, DLD-1, T24, NCI-H1299, and PANC-1) or WT RAS (HT-29 and HeLa) were treated with the indicated compounds for up to 6 days. Cell number was estimated by crystal violet dye retention (see Methods). (**B**) HCT-116 cells with WT K-RAS are resistant to D4476:CQ. Isogenic HCT-116 cells (with/without mutant K-RAS; n = 3 per cell line) were treated as in **A**.

govern the abundance of nuclear FOXO3A proteins and therefore the expression of FOXO3A-responsive genes that are critical for the initiation of autophagy. This is consistent with the observation that phosphoregulation of transcription factors and coregulators by the CK1 family is critical for the tight control of diverse biological process such as circadian rhythm, DNA damage response, and WNT signaling (21). Since no activating mutation in *H-*, *K-*, or *N-RAS* is found in MCF-7 cells, the work of Szyniarowski et al. (20) may be interpreted as basal autophagy being regulated by CK1α even in the absence of hyperactivation of RAS signaling. However, a study indicated that RAS proteins remain highly expressed in MCF-7 cells (52), and this may bypass the need to acquire activating mutations of RAS to facilitate CK1α-dependent control of autophagy induction. Hence, we speculate that CK1α is engaged by the hyperactivated RAS signaling to modulate its resultant autophagic response regardless of whether it is induced by oncogenic mutations or overexpression of RAS proteins.

Last, we report the elucidation of a regulatory mechanism that governs the expression of CK1α. Until recently, CK1α was considered to be a "rogue" kinase (36), as its catalytic activity appears to be unregulated. However, fresh perspectives on the regulation of CK1α were gained in two recent studies, one showing CK1α protein expression to be downregulated by miR-155 in liposarcoma (53) and the other identifying a subset of the DDX family of RNA helicase as essential kinase-stimulatory cofactors of multiple CK1 isoforms, including CK1α (36). We demonstrate that oncogenic RAS, via its PI3K/AKT/mTOR effector pathway, can also increase CK1α protein abundance and function. Such oncogene-induced regulation of CK1α abundance appears to be highly specific, as oncogenic RAS does not alter the abundance of CK1δ and CK1ε. Although CK1δ has been shown to phosphorylate FOXO proteins in vitro (32), our data suggest that CK1α, not CK1δ or CK1ε, phosphorylates FOXO3A to destabilize FOXO3A and suppress FOXO3A-mediated autophagy-related gene transactivation in vivo. Thus, we postulate that CK1α serves as a context-specific brake of the PI3K/AKT/mTOR effector pathway of RAS signaling to curb the hyperactivation of autophagy, which may result in undesirable cytotoxicity. In addition, since the closely related FOXO1 has also been implicated in the induction of autophagy (54–57), CK1α may employ a multipronged approach to suppress autophagy via phosphoregulation of FOXO1 as well. We note that CK1α transcript abundance is reproducibly downregulated upon siRNA-mediated depletion of FOXO3A (Figure 4H). We speculate that the transcriptional control of CK1α expression by FOXO3A may have evolved as yet another late feedback mechanism for FOXO3A to regulate itself.

In summary, our study identifies a critical oncogenic RAS–induced negative feedback loop that requires CK1α. Inhibition of this kinase, combined with clinically approved autophagy inhibitors, produces cell death in vitro and in vivo. The ability to target an essential pathway in RAS-dependent tumors by this paired therapy provides a new approach to these common cancers.

Methods

Plasmid DNA, cell culture, and other reagents. The creation and use of HA-tagged CK1 expression constructs pcDNA3.1-CK1α-3HA, pCEP-4HA-CK1δ, and pCEP-4HA-CK1ε have been previously described (58, 59). The N-terminal myc-tagged CK1α expression construct pCS2-6MT-CK1α was created by reverse transcription–PCR (RT-PCR) amplification of the open reading frame of CK1α from BJ human foreskin fibroblasts and subcloning into the C terminus of myc epitope tags of pCS2-6MT expression vectors. The creation and use of pECE-HA-FOXO3A and pECE-FOXO3A^{S315A} have been previously described (60). The amino N-terminal HA-tagged CK1α (pCLneo-HA-CK1α) was a gift from Nicolas Bidere

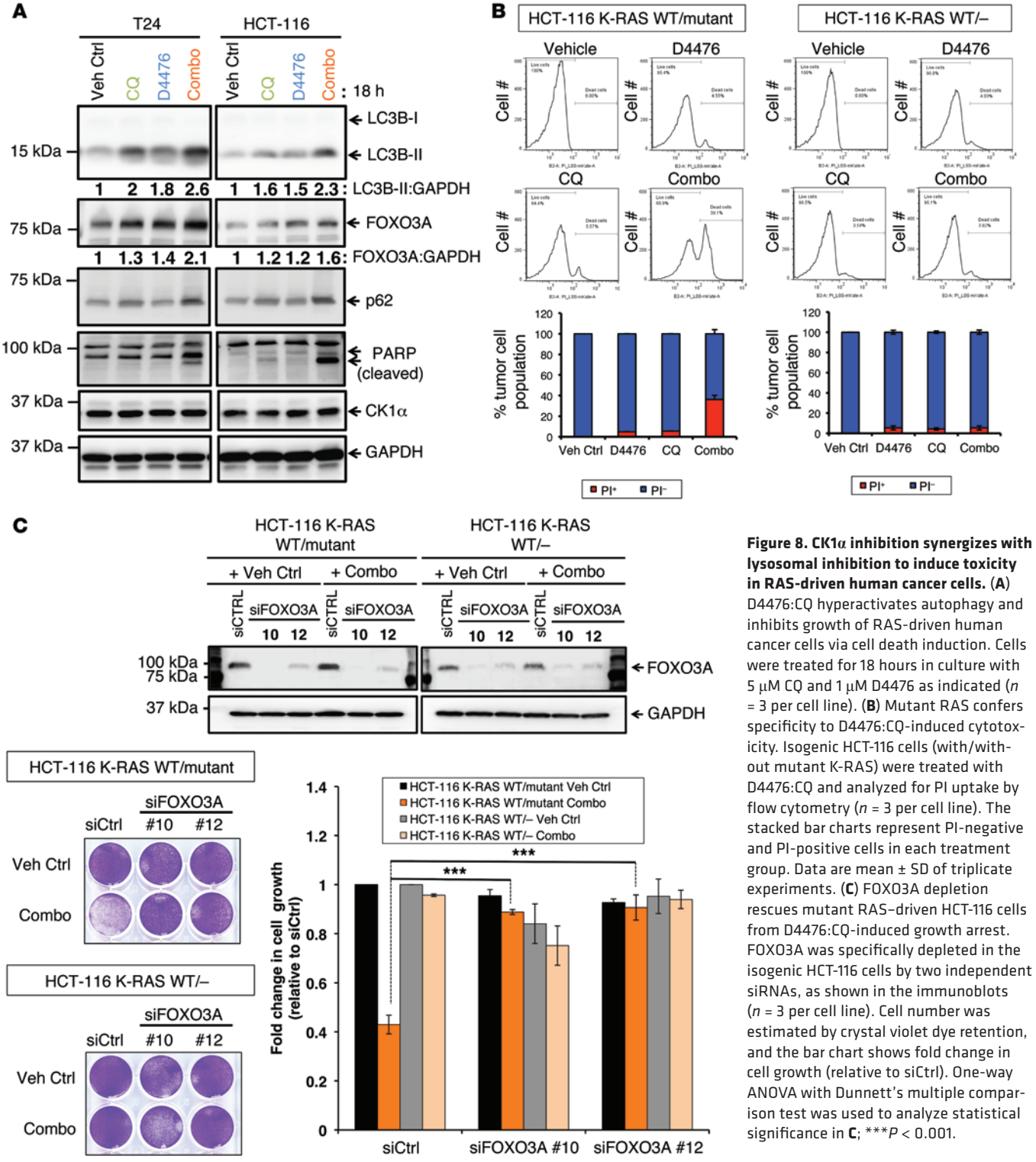

Figure 8. CK1α inhibition synergizes with lysosomal inhibition to induce toxicity in RAS-driven human cancer cells. (**A**) D4476:CQ hyperactivates autophagy and inhibits growth of RAS-driven human cancer cells via cell death induction. Cells were treated for 18 hours in culture with 5 μM CQ and 1 μM D4476 as indicated (n = 3 per cell line). (**B**) Mutant RAS confers specificity to D4476:CQ-induced cytotoxicity. Isogenic HCT-116 cells (with/without mutant K-RAS) were treated with D4476:CQ and analyzed for PI uptake by flow cytometry (n = 3 per cell line). The stacked bar charts represent PI-negative and PI-positive cells in each treatment group. Data are mean ± SD of triplicate experiments. (**C**) FOXO3A depletion rescues mutant RAS–driven HCT-116 cells from D4476:CQ-induced growth arrest. FOXO3A was specifically depleted in the isogenic HCT-116 cells by two independent siRNAs, as shown in the immunoblots (n = 3 per cell line). Cell number was estimated by crystal violet dye retention, and the bar chart shows fold change in cell growth (relative to siCtrl). One-way ANOVA with Dunnett's multiple comparison test was used to analyze statistical significance in **C**; $^{***}P < 0.001$.

(INSERM UMR 1014, Hôpital Paul Brousse, Villejuif, France) (61). pCS2-6MT-CK1α (K46A; kinase-dead mutant), pcDNA3.1-CK1α (R13)-3HA (siCK1α13-resistant mutant), pECE-HA-FOXO3A^{S318}, pECE-FOXO3A^{S321A}, and pECE-FOXO3A$^{S318/321A}$ were created by using the QuikChange II XL Site-Directed Mutagenesis (SDM) Kit in accordance with the manufacturer's instructions (Agilent Technologies). The sequence of primers used for SDM are provided in Supplemental Table 3. The BJ human foreskin fibroblast variants and isogenic HCT-116 colon cancer cell lines (*TP53*-null/*TP53* WT) were gifts from Mathijs Voorhoeve (Duke-NUS) (62) and Bert Vogelstein (Johns Hopkins University, Baltimore, Maryland, USA) (63), respectively. X-MAN isogenic HCT-116 colon cancer cell lines (mutant *K-RAS*–null/mutant *K-RAS* WT) were purchased from Horizon Discovery and cultured in accordance with the manufac-

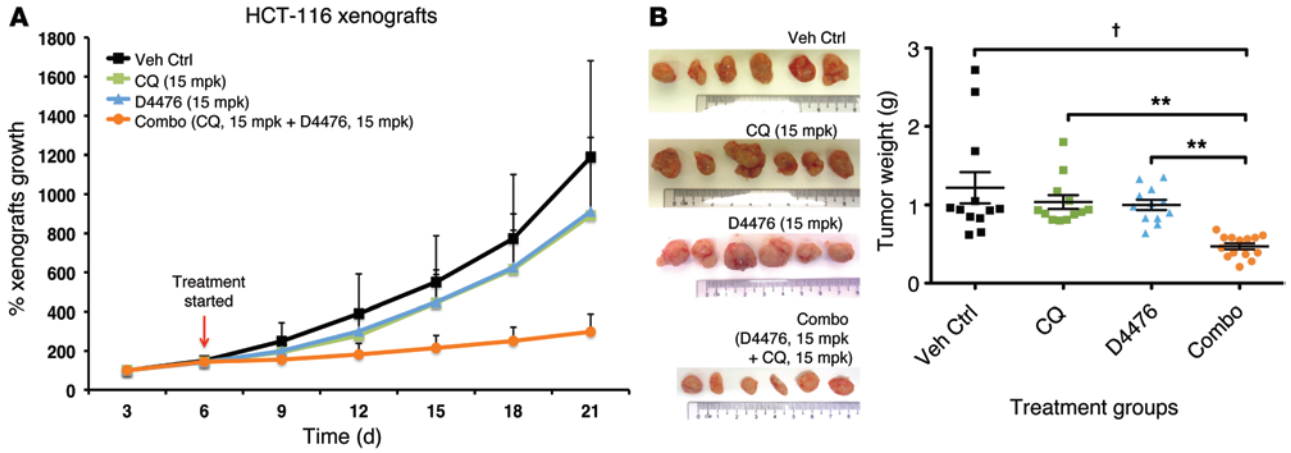

Figure 9. CK1α inhibition synergizes with autophagy inhibition to arrest growth of RAS-driven human cancers. (**A**) D4476:CQ delays HCT-116 tumor xenograft growth. BALB/c athymic nude mice with HCT-116 tumor xenografts were treated with the indicated compounds by daily i.p. injection (n = 6 mice; total of 12 xenografts per treatment group). (**B**) D4476:CQ results in smaller HCT-116 tumor xenografts. Representative images of tumor xenografts in **B** and their respective tumor weights are expressed in a scatter plot (mean ± SD). Two-way ANOVA was used to analyze statistical significance in **B**; $^{**}P < 0.01$; $^{\dagger}P < 0.0001$.

turer's instructions. All other human cancer cell lines used in this study were purchased from ATCC and cultured in accordance with ATCC's instructions. Stabilization and activation of ER:H-RAS^{V12} were achieved by exposing the BJ-derived fibroblasts to 4-OHT (130 nM) for 48–72 hours. For cDNA overexpression studies, jetPRIME transfection reagent (Polyplus Transfection) and X-tremeGENE 9 DNA transfection reagent (Roche) were used to transfect BJ-derived fibroblasts and human cancer cell lines, respectively. Chemical compounds used in this study include 4-OHT (H7904, Sigma-Aldrich), D4476 (D1944, Sigma-Aldrich), PF670462 (PF670; 3316, Tocris Bioscience), PF4800567 (PF480; 4281, Tocris Bioscience), TG (T9033, Sigma-Aldrich), Pyr Pam (P0027, Sigma-Aldrich), CQ (C6628, Sigma-Aldrich), DMSO (D2650, Sigma-Aldrich), SB203850 (S8307, Sigma-Aldrich), LY294002 (L9908, Sigma-Aldrich), U0126 (U120, Sigma-Aldrich), rapamycin (S-015, Sigma-Aldrich), BKM120 (S2247, Selleck Chemicals), and PP242 (S2218, Selleck Chemicals).

Autophagy transcriptome profiling, qPCR, and semi-quantitative RT-PCR analyses. Total RNA was isolated from cultured cells or frozen tumor xenograft tissues using the RNeasy Mini Kit (74106, QIAGEN). Total RNA (2 mg) was reverse transcribed by either the RT^2 HT First Strand Kit (330421, QIAGEN; only for autophagy transcriptome profiling) or the iScript Select cDNA Synthesis Kit (170–8896, Bio-Rad) in accordance with the manufacturer's instructions. Using 1/10 of the cDNA sample, autophagy transcriptome profiling was performed using RT^2 Profiler human autophagy real-time PCR arrays (PAHS-084Z, QIAGEN) and RT^2 SYBR Green qPCR master mixes (330512, QIAGEN). Analysis of autophagy transcriptome profiles was performed using RT^2 Profiler PCR Array Data Analysis v4.0 software (QIAGEN). Using the same amount of cDNA sample and independent primers targeting transcripts of the indicated genes, qPCR was performed by the SsoFast EvaGreen Supermix Kit (172–5200, Bio-Rad) in accordance with the manufacturer's instructions. Semi-quantitative RT-PCRs were performed using 1/10 of the cDNA samples in the presence of 10 mM dNTPs and specific primer pairs (at 10 μM) in a total reaction volume of 20 μl. PCR was performed as follows: 20 cycles of denaturation (94°C, 30 seconds), annealing (51°C, 30 seconds), and extension (72°C, 1 minute), with a 2-minute initial denaturation step at 94°C and a 3-minute terminal polishing step at 72°C. The sequences of primer used for qPCR and semi-quantitative RT-PCR analyses are described in Supplemental Table 3. Expression of *CSNK1A1* (*CK1a*), *CSNK1D* (*CK1δ*), *CSNK1E* (*CK1ε*), *LC3B, BNIP3, ATG12*, *GABARAP*, *ATF4*, *GADD34*, and *GRP78* was quantified using qPCR and normalized to *ACTB* (β-actin) and *HPRT*. Data are presented as fold change relative to vehicle control. Data are mean ± SD of experiments performed in triplicate and representative of 3 independent experiments.

RNAi of human CK1α, CK1δ, CK1ε, FOXO3A, and DDX3 expression. Cells (2×10^5) were plated in 6-well plates and transfected with 100 nM nontargeting siRNA (siCtrl; D-001810-0X) or human CK1α -, CK1δ-, CK1ε-, or FOXO3A-specific siRNAs using DharmaFECT Transfection Reagent (Dharmacon), in accordance with the manufacturer's instructions, for 48–72 hours. The target sequences of human CK1α-, CK1δ-, CK1ε-, and FOXO3A-specific ONTARGETplus siRNAs (Dharmacon RNAi Technologies) were siCK1α13 (J-003957-13): GCGAUGUACUUAAACUAUU; siCK1α14 (J-003957-14): GGAAUCAUUAGGAUAUGUU; siCK1δ18 (J-0034788-18): CGACCUCACAGGCCGACAA; siCK1δ20 (J-003478-20): AGGCUACCCUUCCGAAUUU; siCK1ε11 (J-003479-11): CCUCCGAAUUCUCAACAUA; siCK1ε12 (J-003479-12): CGACUACUCUUACCUACGU; siFOXO3A10 (J-003007-10): GUACUCAACUAGUGCAAAC; and siFOXO3A12 (J-003007-12): UAACUUUGAUUCCCUCAUC. The DDX3-specific siRNAs were synthesized at Singapore Advanced Biologics, and their use has been previously described (36). Cells were transfected with 50 nM DDX3-specific siRNAs using DharmaFECT Transfection Reagent, in accordance with the manufacturer's instructions, for 48–72 hours. The target sequences of human DDX3–specific siRNAs used in this study were siDDX3-1: GCAAAUACUUGGUGUUAGA and siDDX3-2: ACAUUGAGCUUACUCGUUA.

Denaturing SDS-PAGE and WB analyses. Cells were lysed by 4% SDS, and total protein concentration was measured using a bicinchoninic acid protein assay kit (Thermo Scientific). Proteins from whole cell extracts were resolved using denaturing SDS-PAGE and analyzed by WB. Antibodies used in WB analyses include anti-LC3B (2775, Cell Signaling Technology [CST]), anti-RAS (3965, CST),

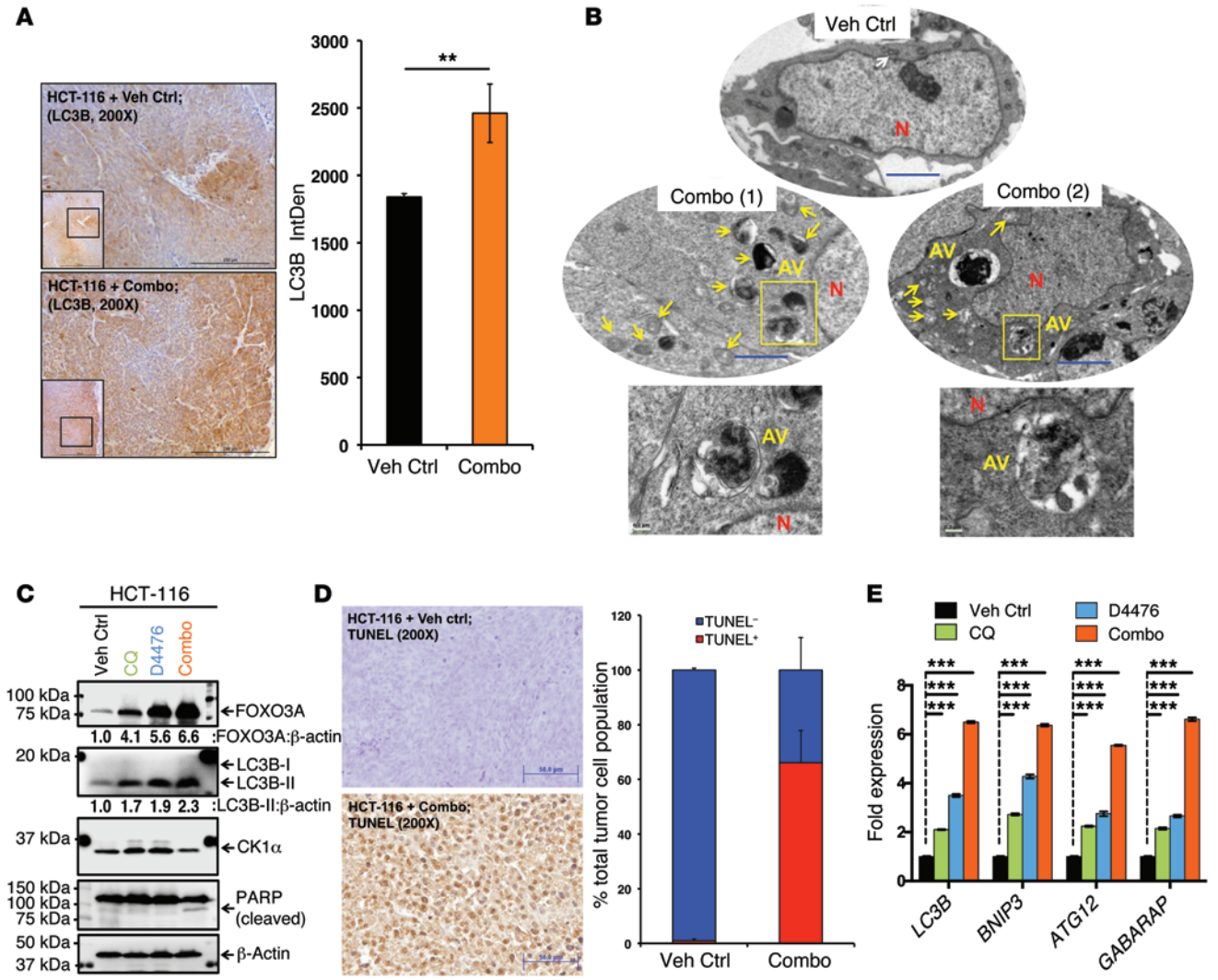

Figure 10. CK1α inhibition synergizes with autophagy inhibition to hyperaccumulate autophagic vesicles and induce cell death in RAS-driven human cancers. (**A**) D4476:CQ elevates LC3B expression in tumor xenografts. LC3B abundance in tumors was assessed by immunostaining and quantitation. A representative section is shown. The insets represent images taken under ×100 magnification in reduced size. Integrated density (IntDen) of LC3B immunostaining in multiple tumor sections (n = 4 per group) was quantified (ImageJ; Student's unpaired t test). Scale bars: 200 μm. (**B**) D4476:CQ induces accumulation of autophagic vesicles (AV) in tumor xenografts. Representative transmission electron micrographs of multiple tumor xenografts are shown. Scale bars: 2 μm (blue), 0.2 μm (insets). Yellow arrows, autophagic vesicles; red N, nucleus; white arrow, mitochondria. (**C**) D4476:CQ upregulates FOXO3A, LC3B-II, and cleaved PARP in tumor xenografts. Representative immunoblots of xenograft lysates are shown. (**D**) D4476:CQ induces cell death in tumor xenografts. Drug-treated tumor xenografts were analyzed by TUNEL staining (see Methods). TUNEL-positive and TUNEL-negative immunostained xenograft sections were quantified (ImageJ), with data shown in the stacked bar chart. Scale bars: 50 μm. Data are mean ± SD of 4 xenografts per group. (**E**) D4476:CQ upregulates FOXO3A-responsive autophagy-related genes. qPCR profiling of xenografts after the indicated therapy is shown. Data are mean ± SD of triplicate experiments and presented as fold expression change relative to controls (1-way ANOVA with Dunnett's test). Fold expression change in the proteins of interest after normalization is shown below protein blots. $^{**}P < 0.01$; $^{***}P < 0.001$.

anti-p53 (DO-1) (sc-126, Santa Cruz Biotechnology Inc.), anti-CK1α (UT3; in-house), anti-CK1α (C-19) (sc-6477, Santa Cruz Biotechnology Inc.), anti-CK1δ (128A, Eli Lilly), anti-CK1ε (610445, BD Biosciences), anti–PP2A A subunit (PP2A/A; JH242; in-house) (64), anti-p62/SQSTM1 (2C11) (H00008878-M01, Novus Biologicals), anti-DDX3 (2635, CST), anti–phospho-FOXO3A$^{S318/321}$ (9465, CST), anti-FOXO3A (75D8) (2497, CST), anti–c-Myc (9E10) (sc-40, Santa Cruz Biotechnology Inc.), anti–HA probe (F7) (sc-7392, Santa Cruz Biotechnology Inc.), anti–Lamin B (sc-6216, Santa Cruz Biotechnology Inc.), anti-GAPDH (2118, CST), anti-Eg5 (4H3-1F12) (4203, CST), anti–β-tubulin (15568, Abcam), anti–β-actin (4967, CST), anti-ATG12 (D88H11) (4180S, CST), anti–phospho-MAPKAPK-2^{T222} (3316, CST), anti–MAPKAPK-2 (12155, CST), anti–phospho-AKT^{S473} (9271, CST), anti-AKT (4691, CST), anti–phospho-ERK$^{T202/Y204}$ (4377, CST), anti-ERK1/2 (9102, CST), anti–phospho-p70 S6K^{T389} (9234, CST), anti–p70 S6K (2708, CST), and anti-PARP (611038, BD Transduction Laboratories). Immunoblots shown in the accompanying figures are derived from three independent experiments. Loading controls used in the WB analyses included PP2A/A, GAPDH, Eg5, β-actin, CK1δ, ERK1/2, AKT, and p70 S6K. Intensities of protein bands were quantified by densitometry (ImageJ; http://imagej.nih.gov/ij/). Numbers below protein blots refer to expres-

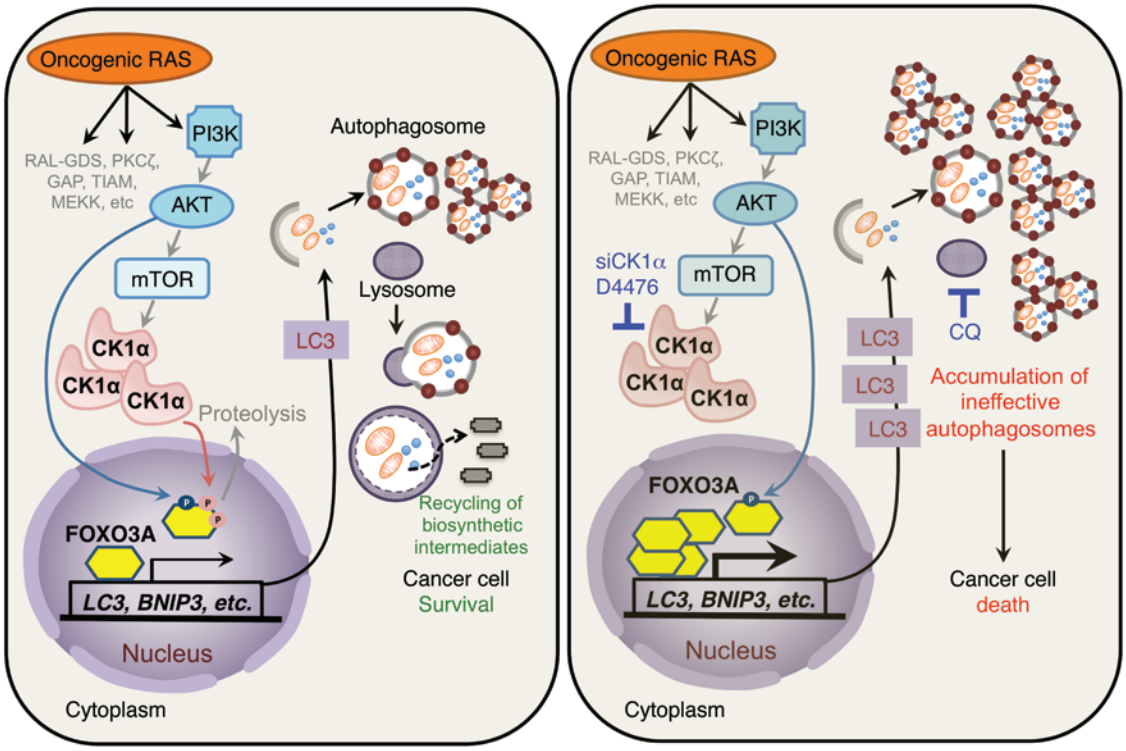

Figure 11. Model of CK1α-mediated regulation of oncogenic RAS–induced autophagy. Left: Oncogenic RAS, via its downstream PI3K/AKT/mTOR effector pathway, increases CK1α protein abundance to prevent hyperactivation of oncogenic RAS–induced autophagy. CK1α phosphorylates FOXO3A at serine residues 318 and 321 to destabilize FOXO3A, decreasing expression of autophagy genes and limiting autophagic recycling of nutrients. Right: RNAi depletion or pharmacological inhibition of CK1α activity by D4476 stabilizes FOXO3A to elevate basal autophagy and autophagic flux. D4476 sensitizes oncogenic RAS–driven cancer cells to lysosomotropic agents (such as CQ and NH_4Cl) via hyperaccumulation of ineffective autophagic vesicles.

sion levels normalized to their loading controls and then calculated as fold expression change relative to treatment controls.

Immunocytochemistry and immunoprecipitation. For immunocytochemistry assays, cells were grown to 50% confluence on glass coverslips in a 12-well tissue culture plate overnight. They were subsequently treated with the indicated siRNAs or chemical compounds at the indicated concentrations for the stated durations. They were washed three times with 1× PBS, fixed in pre-chilled 4% paraformaldehyde for 20 minutes, permeabilized in 0.1% Triton X-100 for 10 minutes, and blocked with 3% BSA for 1 hour. Primary immunostaining with LC3B antibody (2775, CST) or CK1α antibody (UT3; in-house) was performed at room temperature for 1 hour, followed by immunostaining with Alexa Fluor 594–conjugated secondary antibody (Invitrogen). Cellular DNA was subsequently counterstained with DAPI-VECTASHIELD (H-1200, Vector Laboratories). Staining was visualized and photographed using an LSM710 laser scanning confocal microscope with a ×63 oil immersion lens (Zeiss).

Quantitation of LC3B foci–stained cells. Cell images obtained from confocal microscopy were converted to 16-bit monochromatic, grayscale, single-channel images prior to analysis using MetaMorph Microscopy Automation & Image Analysis software (Molecular Devices). The MetaMorph multi-wavelength Cell Scoring application was used on representative images to obtain optimized parameters for cell bodies, as well as nuclear and cytoplasmic stains. All images were then analyzed using the optimized parameters. Cell images were independently validated by performing cell counting on five different magnification fields per image: % LC3B foci–stained cells per image = (number of LC3B foci–containing cells/total number of cells) × 100% in all fields counted.

Subcellular fractionation. Subcellular fractionation of cells was performed using the NE-PER Nuclear and Cytoplasmic Extraction Kit (PI-78835, Thermo Scientific) in accordance with the manufacturer's instructions.

Crystal violet staining. Cells were washed twice in 1× PBS and fixed with methanol for 10 minutes. They were then stained with 0.5% crystal violet dye (in methanol/deionized water, 1:5) for 10 minutes. Excess crystal violet dye was removed by five washes of deionized water on a shaker (10 minutes per wash), and the culture plates were dried overnight. The crystal violet dye was released from cells by incubation with 1% SDS for 6 hours before optical density (OD) 595 nm measurement using a microplate absorbance reader (Bio-Rad).

Flow cytometry cell death analysis. Analysis of apoptosis by propidium iodide (PI) staining and flow cytometry has been previously described (65). In three independent experiments performed in triplicate, 30,000 cells from each treatment group were analyzed via flow cytometry for PI uptake as a result of loss of membrane integrity in apoptotic cells.

alamarBlue cell viability assay and drug combination studies. HCT-116 and T24 human cancer cells (5,000 cells/well) were plated in 96-well tissue culture plates and then treated with escalating doses of each drug for 72 hours. Cell proliferation was assayed after drug treatment by the reduction of alamarBlue reagent (DAL1025,

Invitrogen) (66). Drug combination studies were performed using the method of Chou and Talalay (48). Briefly, the concentrations of D4476 and CQ required to slow cell proliferation by 50% (IC_{50}) were determined in the single-arm experiments. Cells were then treated with increasing doses of D4476 or CQ or an equipotent constant-ratio combination of both drugs. The CIs at 50%, 75%, and 90% growth inhibition, as well as the drug dose-effect curves, were calculated using CalcuSyn software (Biosoft). CI values less than 1, equal to 1, and more than 1 indicate synergism, additive effect, and antagonism, respectively.

Murine xenograft assays. BALB/c athymic nude mice (*nu/nu*) purchased from InVivos were kept under specific pathogen–free (SPF) conditions. Ten million HCT-116 colon cancer cells or T24 bladder cancer cells were mixed with BD Matrigel matrix (1:1; BD Biosciences) and injected subcutaneously into the flanks of 6-week-old athymic nude mice (n = 6 mice in each treatment group bearing HCT-116 xenografts; n = 3 mice in each treatment group bearing T24 xenografts). Mice were examined daily for tumor engraftment after tumor cell injection. Weight of mice and tumor dimensions were measured daily from day 3 after tumor cell injection. Tumor ellipsoid volume was estimated using previously described formulas (67). Mice bearing HCT-116 xenografts were injected i.p. with 150 μl vehicle control (Veh Ctrl: 30% PEG in 0.9% saline), 15 mpk D4476, 15 mpk CQ, or 15 mpk:15 mpk D4476:CQ daily for 15 days. Mice bearing T24 xenografts were injected i.p. with 150 μl vehicle control (30% PEG in 0.9% saline), 5 mpk D4476, 30 mpk D4476, 15 mpk CQ, or 5 mpk:15 mpk D4476:CQ daily for 9 days. Percent increase in xenograft growth is a measure of tumor ellipsoid volume at time points after the commencement of drug treatment (from day 6) relative to the time point of the last treatment of the naive group (day 3). Mice were sacrificed at the end of the treatment schedule, and all tumors were harvested for immunohistochemical, WB, and qPCR analyses.

Immunohistochemical assays. Antigens were retrieved from formaldehyde-fixed, paraffin-embedded (FFPE) tumor tissue sections by 30 minutes boiling in sodium citrate buffer (pH 6.0) using a microwave histoprocessor (Milestone). Endogenous peroxidase activity in tissue sections was depleted by treatment with 3% hydrogen peroxide (H_2O_2; in 1× TBS) for 20 minutes at room temperature. Immunohistochemical staining was performed by incubating the antigen-retrieved FFPE tumor tissue sections using rabbit LC3B (D11) XP primary antibody (3868, CST; 1:200 in 3% BSA/TBS–Tween 20) overnight at 4°C with gentle shaking. This was followed by incubation with goat anti–rabbit HRP secondary antibody (170-6515, Bio-Rad; 1:200 in 3% BSA/TBS) for 1 hour at room temperature. The immunostained sections were then exposed to DAB substrate (dissolved in Dako substrate buffer, 34680), followed by Gill's hematoxylin counterstaining and standard dehydration treatment. Coverslips were mounted onto these sections using xylene-based mounting medium (44581, Sigma-Aldrich DPX Mountant for histology). Staining was visualized using a Leica DM 2000 microscope. The integrated density (IntDen) of LC3B expression in the tumor xenograft sections was quantified by densitometry (ImageJ).

TUNEL assay. Apoptotic DNA strand breaks were detected by TUNEL staining of paraffin-embedded tumor xenograft sections in accordance with the protocol for the ApopTag Peroxidase In Situ Apoptosis Detection Kit (S7100, Millipore) and coverslipped using DPX Mountant. Staining was visualized using an Olympus IX71S1F3 microscope. TUNEL-negative and TUNEL-positive tumor cells in the xenograft sections were quantified using the cell counter plugin of ImageJ software.

Transmission electron microscopy. Tissue specimens were processed for transmission electron microscopy (TEM) and analyzed by a histopathologist blinded to the treatment arms. Samples were first fixed in 2% paraformaldehyde and 4% glutaraldehyde overnight and postfixed in 1% osmium tetroxide (pH 7.4) for 2 hours at room temperature. Specimens were then dehydrated through an ascending series of ethanol baths, infiltrated with acetone and resin, and then embedded in Araldite 502 (18052, Ted Pella Inc.). Ultrathin sections were cut using an ultramicrotome and mounted on Formvar-coated copper grids (24915, Polysciences Inc.). Sections were then double stained with uranyl acetate and lead citrate. TEM images of the sections were taken using a JEOL JEM-1010 Transmission Electron Microscope.

Statistics. Statistical significance in experiments was assessed using GraphPad Prism, version 5 (GraphPad Software). Student's unpaired, 2-tailed t tests with a 95% confidence interval were used to analyze data involving direct comparison of an experimental group with a control group. One-way ANOVA tests with Dunnett's method for multiple comparisons with a 95% confidence interval were used to analyze data involving two or more test groups and a control group; two-way ANOVA tests for multiple comparisons with a 95% confidence interval were used to analyze data obtained from the assessment of drug synergy on tumor xenograft growth. Reported P values were adjusted to account for multiple comparisons. A P value less than 0.05 was considered statistically significant.

Study approval. The care and use of BALB/c athymic nude mice (*nu/nu*) was approved by the Duke-NUS IACUC, in accordance with protocol 2011/SHS/693.

Acknowledgments

We thank Jamal Aliyev, Kakaly Ghosh, Edison, Daniel Yim, and Ha Yin Lee (Duke-NUS) for excellent technical support. We also thank Ya Jun Wu (NUS) for technical assistance with electron microscopy. We are greatly indebted to Christopher Counter (Duke University) and our NUS/Duke-NUS colleagues Shing Leng Chan, Shazib Pervaiz, Mei Wang-Casey, Sharon Lim, Wei Zhou, and John Allen, as well as all members of the Virshup laboratory for reagents and helpful discussions. We are grateful to Wai Leong Tam (Massachusetts Institute of Technology) for critically reading the manuscript. This work was supported by the Duke-NUS Signature Research Program funded by the Agency for Science, Technology and Research, Singapore; the Ministry of Health, Singapore; and a Singapore Translational Research Investigator Award to D.M. Virshup funded by the National Research Foundation and the National Medical Research Council (NMRC; NMRC/STaR/R-913-301-006-213). J.K. Cheong was supported by an NMRC–Cooperative Basic Research Grant (NMRC-CBRG) New Investigator Grant (NMRC/BNIG/1078/2012).

Address correspondence to: David M. Virshup or Jit Kong Cheong, Cancer and Stem Cell Biology Program, Duke-NUS Graduate Medical School Singapore, 8 College Road, 169857, Singapore. Phone: 65.65166954; E-mail: david.virshup@duke-nus.edu.sg (D.M. Virshup), jitkong.cheong@duke-nus.edu.sg (J.K. Cheong).

1. Bray F, Jemal A, Grey N, Ferlay J, Forman D. Global cancer transitions according to the Human Development Index (2008–2030): a population-based study. *Lancet Oncol*. 2012;13(8):790–801.
2. Downward J. Targeting RAS signalling pathways in cancer therapy. *Nat Rev Cancer*. 2003;3(1):11–22.
3. Elgendy M, Sheridan C, Brumatti G, Martin SJ. Oncogenic Ras-induced expression of Noxa and Beclin-1 promotes autophagic cell death and limits clonogenic survival. *Mol Cell*. 2011;42(1):23–35.
4. Guo JY, et al. Activated Ras requires autophagy to maintain oxidative metabolism and tumorigenesis. *Genes Dev*. 2011;25(5):460–470.
5. Kim MJ, et al. Involvement of autophagy in oncogenic K-Ras-induced malignant cell transformation. *J Biol Chem*. 2011;286(15):12924–12932.
6. Lock R, et al. Autophagy facilitates glycolysis during Ras-mediated oncogenic transformation. *Mol Biol Cell*. 2011;22(2):165–178.
7. Yang S, et al. Pancreatic cancers require autophagy for tumor growth. *Genes Dev*. 2011;25(7):717–729.
8. Slattum G, Gu Y, Sabbadini R, Rosenblatt J. Autophagy in oncogenic K-Ras promotes basal extrusion of epithelial cells by degrading S1P. *Curr Biol*. 2014;24(1):19–28.
9. Guo JY, et al. Autophagy suppresses progression of K-ras-induced lung tumors to oncocytomas and maintains lipid homeostasis. *Genes Dev*. 2013;27(13):1447–1461.
10. Lock R, Kenific CM, Leidal AM, Salas E, Debnath J. Autophagy-dependent production of secreted factors facilitates oncogenic RAS-driven invasion. *Cancer Discov*. 2014;4(4):466–479.
11. Gump JM, Thorburn A. Autophagy and apoptosis: what is the connection? *Trends Cell Biol*. 2011;21(7):387–392.
12. Barnard RA, Wittenburg LA, Amaravadi RK, Gustafson DL, Thorburn A, Thamm DH. Phase I clinical trial and pharmacodynamic evaluation of combination hydroxychloroquine and doxorubicin treatment in pet dogs treated for spontaneously occurring lymphoma. *Autophagy*. 2014;10(8):1415–1425.
13. Mahalingam D, et al. Combined autophagy and HDAC inhibition: a phase I safety, tolerability, pharmacokinetic, and pharmacodynamic analysis of hydroxychloroquine in combination with the HDAC inhibitor vorinostat in patients with advanced solid tumors. *Autophagy*. 2014;10(8):1403–1414.
14. Rangwala R, et al. Combined MTOR and autophagy inhibition: phase I trial of hydroxychloroquine and temsirolimus in patients with advanced solid tumors and melanoma. *Autophagy*. 2014;10(8):1391–1402.
15. Rangwala R, et al. Phase I trial of hydroxychloroquine with dose-intense temozolomide in patients with advanced solid tumors and melanoma. *Autophagy*. 2014;10(8):1369–1379.
16. Rosenfeld MR, et al. A phase I/II trial of hydroxychloroquine in conjunction with radiation therapy and concurrent and adjuvant temozolomide in patients with newly diagnosed glioblastoma multiforme. *Autophagy*. 2014;10(8):1359–1368.
17. Vogl DT, et al. Combined autophagy and proteasome inhibition: a phase 1 trial of hydroxychloroquine and bortezomib in patients with relapsed/refractory myeloma. *Autophagy*. 2014;10(8):1380–1390.
18. Morgan MJ, et al. Regulation of autophagy and chloroquine sensitivity by oncogenic RAS in vitro is context-dependent. *Autophagy*. 2014;10(10):1814–1826.
19. Cheong JK, et al. IC261 induces cell cycle arrest and apoptosis of human cancer cells via CK1δ/ε and Wnt/β-catenin independent inhibition of mitotic spindle formation. *Oncogene*. 2011;30(22):2558–2569.
20. Szyniarowski P, et al. A comprehensive siRNA screen for kinases that suppress macroautophagy in optimal growth conditions. *Autophagy*. 2011;7(8):892–903.
21. Cheong JK, Virshup DM. Casein kinase 1: complexity in the family. *Int J Biochem Cell Biol*. 2011;43(4):465–469.
22. Davidson G, et al. Casein kinase 1 gamma couples Wnt receptor activation to cytoplasmic signal transduction. *Nature*. 2005;438(7069):867–872.
23. Firestein R, et al. CDK8 is a colorectal cancer oncogene that regulates beta-catenin activity. *Nature*. 2008;455(7212):547–551.
24. Gallego M, Virshup DM. Post-translational modifications regulate the ticking of the circadian clock. *Nat Rev Mol Cell Biol*. 2007;8(2):139–148.
25. Knippschild U, Gocht A, Wolff S, Huber N, Lohler J, Stoter M. The casein kinase 1 family: participation in multiple cellular processes in eukaryotes. *Cell Signal*. 2005;17(6):675–689.
26. Price MA. CKI, there's more than one: casein kinase I family members in Wnt and Hedgehog signaling. *Genes Dev*. 2006;20(4):399–410.
27. Liu C, et al. Control of β-catenin phosphorylation/degradation by a dual-kinase mechanism. *Cell*. 2002;108(6):837–847.
28. Huart AS, MacLaine NJ, Meek DW, Hupp TR. CK1α plays a central role in mediating MDM2 control of p53 and E2F-1 protein stability. *J Biol Chem*. 2009;284(47):32384–32394.
29. Hahn WC, Counter CM, Lundberg AS, Beijersbergen RL, Brooks MW, Weinberg RA. Creation of human tumour cells with defined genetic elements. *Nature*. 1999;400(6743):464–468.
30. Scherz-Shouval R, Weidberg H, Gonen C, Wilder S, Elazar Z, Oren M. p53-dependent regulation of autophagy protein LC3 supports cancer cell survival under prolonged starvation. *Proc Natl Acad Sci U S A*. 2010;107(43):18511–18516.
31. Jaras M, et al. Csnk1a1 inhibition has p53-dependent therapeutic efficacy in acute myeloid leukemia. *J Exp Med*. 2014;211(4):605–612.
32. Rena G, Bain J, Elliott M, Cohen P. D4476, a cell-permeant inhibitor of CK1, suppresses the site-specific phosphorylation and nuclear exclusion of FOXO1a. *EMBO Rep*. 2004;5(1):60–65.
33. Denoyelle C, et al. Anti-oncogenic role of the endoplasmic reticulum differentially activated by mutations in the MAPK pathway. *Nat Cell Biol*. 2006;8(10):1053–1063.
34. Milani M, et al. The role of ATF4 stabilization and autophagy in resistance of breast cancer cells treated with Bortezomib. *Cancer Res*. 2009;69(10):4415–4423.
35. Shirasawa S, Furuse M, Yokoyama N, Sasazuki T. Altered growth of human colon cancer cell lines disrupted at activated Ki-ras. *Science*. 1993;260(5104):85–88.
36. Cruciat CM, et al. RNA helicase DDX3 is a regulatory subunit of casein kinase 1 in Wnt-beta-catenin signaling. *Science*. 2013;339(6126):1436–1441.
37. Klionsky DJ, et al. Guidelines for the use and interpretation of assays for monitoring autophagy. *Autophagy*. 2012;8(4):445–544.
38. Mammucari C, et al. FoxO3 controls autophagy in skeletal muscle in vivo. *Cell Metab*. 2007;6(6):458–471.
39. Webb AE, Brunet A. FOXO transcription factors: key regulators of cellular quality control. *Trends Biochem Sci*. 2014;39(4):159–169.
40. Zhao J, et al. FoxO3 coordinately activates protein degradation by the autophagic/lysosomal and proteasomal pathways in atrophying muscle cells. *Cell Metab*. 2007;6(6):472–483.
41. Fullgrabe J, Klionsky DJ, Joseph B. The return of the nucleus: transcriptional and epigenetic control of autophagy. *Nat Rev Mol Cell Biol*. 2014;15(1):65–74.
42. Flotow H, Graves PR, Wang AQ, Fiol CJ, Roeske RW, Roach PJ. Phosphate groups as substrate determinants for casein kinase I action. *J Biol Chem*. 1990;265(24):14264–14269.
43. Thorne CA, et al. Small-molecule inhibition of Wnt signaling through activation of casein kinase 1α. *Nat Chem Biol*. 2010;6(11):829–836.
44. Swiatek W, et al. Regulation of casein kinase I epsilon activity by Wnt signaling. *J Biol Chem*. 2004;279(13):13011–13017.
45. Lee JC, et al. A protein kinase involved in the regulation of inflammatory cytokine biosynthesis. *Nature*. 1994;372(6508):739–746.
46. Bondar VM, Sweeney-Gotsch B, Andreeff M, Mills GB, McConkey DJ. Inhibition of the phosphatidylinositol 3′-kinase-AKT pathway induces apoptosis in pancreatic carcinoma cells in vitro and in vivo. *Mol Cancer Ther*. 2002; 1(12):989–997.
47. Favata MF, et al. Identification of a novel inhibitor of mitogen-activated protein kinase kinase. *J Biol Chem*. 1998;273(29):18623–18632.
48. Chou TC, Talalay P. Quantitative analysis of dose-effect relationships: the combined effects of multiple drugs or enzyme inhibitors. *Adv Enzyme Regul*. 1984;22:27–55.
49. Mizushima N, Komatsu M. Autophagy: renovation of cells and tissues. *Cell*. 2011; 147(4):728–741.
50. Karsli-Uzunbas G, et al. Autophagy is required for glucose homeostasis and lung tumor maintenance. *Cancer Discov*. 2014;4(8):914–927.
51. Hu Y, Song W, Cirstea D, Lu D, Munshi NC, Anderson KC. CSNK1α1 mediates malignant plasma cell survival. *Leukemia*. 2015;29(2):474–482.
52. Omerovic J, Hammond DE, Clague MJ, Prior IA. Ras isoform abundance and signalling in human cancer cell lines. *Oncogene*. 2008; 27(19):2754–2762.
53. Zhang P, et al. MiR-155 is a liposarcoma oncogene that targets casein kinase-1α and enhances β-catenin signaling. *Cancer Res*. 2012;72(7):1751–1762.
54. Hariharan N, Maejima Y, Nakae J, Paik J, Depinho RA, Sadoshima J. Deacetylation of FoxO by Sirt1 plays an essential role in mediating starvation-induced autophagy in cardiac myocytes. *Circ Res*.

2010;107(12):1470–1482.
55. Liu HY, et al. Hepatic autophagy is suppressed in the presence of insulin resistance and hyperinsulinemia: inhibition of FoxO1-dependent expression of key autophagy genes by insulin. *J Biol Chem*. 2009;284(45):31484–31492.
56. Sengupta A, Molkentin JD, Yutzey KE. FoxO transcription factors promote autophagy in cardiomyocytes. *J Biol Chem*. 2009;284(41):28319–28331.
57. Zhao Y, et al. Cytosolic FoxO1 is essential for the induction of autophagy and tumour suppressor activity. *Nat Cell Biol*. 2010;12(7):665–675.
58. Chen L, Li C, Pan Y, Chen J. Regulation of p53-MDMX interaction by casein kinase 1 α. *Mol Cell Biol*. 2005;25(15):6509–6520.
59. Rivers A, Gietzen KF, Vielhaber E, Virshup DM. Regulation of casein kinase I ε and casein kinase I Δ by an in vivo futile phosphorylation cycle. *J Biol Chem*. 1998;273(26):15980–15984.
60. Brunet A, et al. Akt promotes cell survival by phosphorylating and inhibiting a Forkhead transcription factor. *Cell*. 1999;96(6):857–868.
61. Bidere N, et al. Casein kinase 1alpha governs antigen-receptor-induced NF-κB activation and human lymphoma cell survival. *Nature*. 2009;458(7234):92–96.
62. Voorhoeve PM, Agami R. The tumor-suppressive functions of the human INK4A locus. *Cancer Cell*. 2003;4(4):311–319.
63. Bunz F, et al. Disruption of p53 in human cancer cells alters the responses to therapeutic agents. *J Clin Invest*. 1999;104(3):263–269.
64. McCright B, Virshup DM. Identification of a new family of protein phosphatase 2A regulatory subunits. *J Biol Chem*. 1995;270(44):26123–26128.
65. Riccardi C, Nicoletti I. Analysis of apoptosis by propidium iodide staining and flow cytometry. *Nat Protoc*. 2006;1(3):1458–1461.
66. Nakayama GR, Caton MC, Nova MP, Parandoosh Z. Assessment of the Alamar Blue assay for cellular growth and viability in vitro. *J Immunol Methods*. 1997;204(2):205–208.
67. Tomayko MM, Reynolds CP. Determination of subcutaneous tumor size in athymic (nude) mice. *Cancer Chemother Pharmacol*. 1989;24(3):148–154.